Structural Decomposition of Merger-Free Galaxies Hosting Luminous AGN

Matthew J. Fahey

Physics

Department of Physics

Lancaster University

Date

02/10/2022

A thesis submitted to Lancaster University for the degree of Master of Physics by Research

Supervised by

Brooke D. Simmons

Abstract

Black hole-galaxy co-evolution is a cornerstone of modern extragalactic astrophysics. Previous work has suggested galaxy mergers are the primary mechanism through which co-evolution occurs, growing the mass of both galaxies and their black holes. More recent observational studies have called this concept into question, proposing merger free pathways for black hole-galaxy co-evolution. We investigate a sample of disk-dominated galaxies hosting luminous AGN and structurally decompose them using `GALFIT` to reveal their morphological components. We detect a classical bulge component in $53.3 \pm 0.5\%$ of the galaxies in our sample, however we find these galaxies are still unambiguously disk-dominated, with an average B/Tot for the entire sample of 0.1 ± 0.1. We find galaxies hosting only bulges host overly massive black holes and more luminous AGN in comparison to galaxies hosting only pseudobulges, though we also find evidence that mergers are not a requirement to grow black holes to supermassive size. We investigate the barred fraction of our sample and find that galaxies hosting bars host neither overly massive black holes, nor overly luminous AGN, suggesting the presence of a bar is not a requirement to grow black holes to supermassive size in the local Universe in the absence of major mergers. Considering black hole-galaxy mass relations we find some correlation between bulge mass and black hole mass for disk-dominated galaxies, though we note that this correlation is significantly weaker in comparison to the relation for bulge-dominated galaxies. Furthermore, a significant fraction ($\gtrsim 90\%$) of these black holes are overly massive when compared to this canonical relation. We find a similar correlation between total stellar mass and black hole mass for the disk-dominated galaxies, and

investigate the extent to which these findings indicate differences in the stochasticity of black hole-galaxy co-evolution in disk-dominated versus bulge-dominated systems.

For Ann

Acknowledgements

The author would like to thank K. Wiersema, D. O'Ryan, I. Garland, M. Thorne, A. Mohammed, D. Kuzin, T. Cornish, and H. Wade for the numerous enlightening discussions related to this work, as well as C. Peng and the `GALFIT` News and Discussion Forum for their guidance and support.

The author would also like to thank his supervisor, B. Simmons, without whom this work would not have been possible.

In addition to the computer software cited in the manuscript below, the author has benefited immensely from the publicly available programming language `Python`, including `NumPy` (Van Der Walt et al., 2011), `SciPy` (Jones et al., 2001), `Matplotlib` (Hunter, 2007) and `astroPy` (Astropy Collaboration et al., 2013). He also made extensive use of NASA's Astrophysics Data System (ADS), Cornell University's arXiv, the JavaScript Cosmology Calculator (Wright, 2006), and the Tool for Operations on Catalogues and Tables (`Topcat`, Taylor, 2013).

Declaration

This thesis is my own work and no portion of the work referred to in this thesis has been submitted in support of an application for another degree or qualification at this or any other institute of learning.

It is far better to grasp the Universe as it really is than to persist in delusion, however satisfying and reassuring.

- Carl Sagan

Everybody that I've ever seen that enjoyed their job was very good at it.

- Charles "Chuck" Yeager

Contents

List of Figures

Chapter 1

Introduction

Strong correlations observed between the masses of supermassive black holes (SMBHs) and galaxy properties such as velocity dispersion, (see e.g., Ferrarese & Merritt, 2000, Kormendy & Gebhardt, 2001, Magorrian et al., 1998); bulge stellar mass, (see e.g., Häring & Rix, 2004, Marconi & Hunt, 2003) and total stellar mass, (see e.g., Cisternas et al., 2011, Marleau et al., 2013) have led to the growing consensus that galaxies engage in a process of co-evolution with the SMBHs they host (for a thorough review see Kormendy & Ho, 2013).

Any theory of galaxy growth and evolution must endeavour to explain these correlations, and as such the role played by galaxy mergers has emerged as a prominent area of research, with previous literature pointing to major mergers as the primary mechanism through which a galaxy can grow both its stellar and black hole mass (see e.g., Croton et al., 2006, Hopkins et al., 2006, Peng, 2007, Sanders et al., 1988).

Galaxy mergers are a key process through which stars can be transferred from rotation-supported structures such as galactic disks to dispersion-supported structures such as bulges and elliptical galaxies (see e.g., Hopkins et al., 2012, Walker et al., 1996, Welker et al., 2017). Numerical simulations of merging galaxies suggest that their gas content is subject to a significant gravitational torque (Barnes & Hernquist, 1996, Hernquist, 1989), and this violent process involves substantial angular momentum transfer which can act to funnel gas from kiloparsec-scale to parsec-scale orbits. This global gas transfer allows increased volumes of gas to be accreted onto a central SMBH, triggering an active galactic nucleus (AGN; Shlosman et al., 1989).

The morphology of a given galaxy contains artefacts which hint to its long-term evolution. When considering gas-rich disk galaxies, while it is possible for disks to re-form following a major merger event (see Emsellem et al., 2011, Hopkins et al., 2009, Pontzen et al., 2017, Sparre & Springel, 2017), a central classical bulge component often remains as a relic in the post-merger structure. The minimum galaxy mass ratio required for a merger event to create a bulge is routinely cited as 1:10 (Hopkins et al., 2012, Tonini et al., 2016, Walker et al., 1996), though recent theoretical studies have introduced some uncertainty into this number (Brook et al., 2012, Hopkins et al., 2009, Kannan et al., 2015).

In the context of merger-driven galaxy evolution it is also of paramount importance to make the distinction between the classical, dispersion supported bulge components predominantly formed through the merger events mentioned above, and visually similar but dynamically different pseudobulge components. Whilst pseudobulges may appear visually indistinguishable from classical bulge components, these pseudobulges are still rotation supported structures, and have likely grown through purely secular processes (Kormendy & Kennicutt, 2004, Kormendy et al., 2010). Hence, we can also consider galaxies whose only compact components are pseudobulges as identical to pure disk-galaxies.

Furthermore, additional work has suggested that classical bulges may form and grow through processes other than mergers (Bell et al., 2017, Guo et al., 2020, Park et al., 2019, Sales et al., 2012, Scannapieco et al., 2009, Wang et al., 2019, Zolotov et al., 2015). This growing body of work points to the conclusion that galaxies which are unambiguously disk-dominated in their morphologies have likely had an extremely calm baryon accretion history, evolving in the absence of major mergers since $z \sim 2$ (Martig et al., 2012).

If major mergers are indeed the primary driver of galaxy-black hole correlations, then we should expect that black hole properties should correlate almost exclusively with galaxy properties tied to merger histories, and not with properties which develop in the absence of mergers. Some past studies support these findings (Kormendy & Bender, 2011, Kormendy et al., 2011), and it has been found that luminous quasars seem preferentially hosted in ongoing mergers (Glikman et al., 2015, Trakhtenbrot et al., 2017, Urrutia et al., 2008, Volonteri & Rees, 2006). Studies also suggest AGN triggering due to major merger events (Bessiere et al., 2014, Gao et al., 2020, Treister et al., 2012) with additional evidence suggesting AGN activity peaks post-merger (Ellison et al., 2013, Schawinski et al., 2010).

However, recent observational studies have cast increasing doubt on the relevance of major mergers for triggering AGN activity and facilitating black-hole galaxy co-evolution. When considering vast numbers of X-ray detected and optically observed AGN across cosmic time, no significant connection between merger driven triggering and fuelling could be found (Cisternas et al., 2011, Gabor et al., 2009, Georgakakis et al., 2009). Furthermore, moderate luminosity AGN which represent more typical rates of black hole growth (Hasinger et al., 2005) show an almost identical trend: that there is no observational connection between the triggering and fuelling of AGN by major mergers (Allevato et al., 2011, Cisternas et al., 2015, Goulding et al., 2017, Grogin et al., 2005, Kocevski et al., 2012, Marian et al., 2019, Rosario et al., 2015, Schawinski et al., 2011, Silva et al., 2021).

In addition, simulations have suggested that whilst mergers may increase the rate of luminous AGN, they do not play a significant role in driving black hole growth (McAlpine et al., 2020), with Martin et al. (2018) suggesting that as little as $\sim 35\%$ of black hole growth since $z \sim 3$ can be traced back to merger induced fuelling, both major and minor.

Merger-free pathways for black hole-galaxy co-evolution have been hypothesised in the past (Cisternas et al., 2011, Greene et al., 2010, Jiang et al., 2011, Simmons et al., 2013), and there is increasing evidence that merger-free processes such as galactic bars (Ann & Thakur, 2005, Athanassoula, 2003, Friedli & Benz, 1993) or purely calm 'secular' processes (Kormendy & Kennicutt, 2004) might be viable options for growing SMBHs.

Smethurst et al. (2019) investigate possible powering mechanisms for their population of disk-dominated AGN selected from the parent sample of Simmons et al. (2017). Having calculated a mean mass inflow rate of 1.01 ± 0.14 $M_{\odot}$ yr^{-1} they show that simulations indicate morphological features such as bars (Lin et al., 2013, Maciejewski et al., 2002, Regan & Teuben, 2004, Sakamoto, 1996) and spiral arms (Davies et al., 2009, Maciejewski, 2004, Schnorr-Müller et al., 2014), as well as smooth accretion of cold gas (Kereš et al., 2005, Sancisi et al., 2008) can each match this required rate, and hence should be capable of sustainably fuelling an AGN. Furthermore, as morphological features such as bars and spiral arms are thought to be long lasting (D'Onghia et al., 2013, Donner & Thomasson, 1994, Hunt et al., 2018, Miller & Smith, 1979, Sparke & Sellwood, 1987) it is feasible these inflow rates can be sustained in the long term, implying purely secular growth processes can rapidly grow SMBHs.

However, due to the relative rarity of merger-free galaxies hosting luminous AGN, previously studied samples have routinely suffered from issues such as: being too small to statistically constrain black-hole galaxy relations dependent on merger-free pathways, making use of selection techniques that preclude sampling the full parameter space of galaxy and black-hole mass, and including obscured AGN for which the only available black-hole mass estimation frameworks are highly uncertain. While recent work has vastly improved upon these issues, a lack of high resolution imaging has placed a fundamental upper limit on the extent to which any observed correlations could be constrained. Previous work has pointed to the importance of parametric image fitting for decomposing galaxy morphology (Kim et al., 2008, Pierce et al., 2010, Simmons & Urry, 2008) and as such, high quality imagery, such as that from the *Hubble Space Telescope* (*HST*), is required for an independent assessment of host morphology and to quantify bulge contribution.

In this work we present a sample of 101 luminous, unobscured AGN hosted in disk-dominated galaxies imaged with *HST*. We make use of the 2D paramteric image fitting software `GALFIT` (Peng et al., 2002, 2010) to structurally decompose each of these galaxies, classifying each component individually and making clear distinctions between classical bulges and pseudobulges. We investigate the extent to which galaxies hosting bulges differ from the overall population, and explore the mechanisms by which these differences might be explained.

In Chapter 2 we describe the observational data and the selection of disk dominated galaxies hosting luminous AGN. In Chapter 3 we describe the methods used to structurally decompose these sources using `GALFIT` and the schemes used for component classification. In Chapter 4 we outline the calculation of additional sample parameters to better inform our analysis including luminosity ratios, galaxy stellar masses, and black hole masses. In Chapter 5 we investigate the barred fraction of our galaxies in detail. In Chapter 6 we investigate black hole-galaxy relations and black hole-galaxy co-evolution. Our findings are summarised in Chapter 7.

Throughout this paper all cross-matched catalogues use the nearest positional match to within 3". We use the AB magnitude system (Oke & Gunn, 1983) and we adopt the following flat ΛCDM cosmology: $H_0 = 70.0$ kms^{-1}Mpc^{-1}, $\Omega_M = 0.3$ and $\Omega_\Lambda = 0.7$.

Chapter 2

Observational Data

This work concerns data that were initially selected in the parent sample of Simmons et al. (2017). An initial AGN sample was composed using the W2R sample of Edelson & Malkan (2012). This selection was performed utilising infrared colours in addition to X-ray information to select unobscured AGN at high confidence. Further use of the Sloan Digital Sky Survey (SDSS; York et al., 2000) enabled the selection from this initial sample of a sample of AGN that have disk-dominated morphologies. This selection involved morphological classification by a single expert classifier (BDS), identifying 137 systems where disk features (e.g. spiral arms, bars etc.) were obvious but bulge features were absent.

As the aims of Simmons et al. (2017) were to investigate black hole growth in galaxies which have evolved in the absence of major mergers, their focus was on selecting a sample of luminous AGN that were also hosted in galaxies with morphologies that are unambiguously disk-dominated. As such, the luminosity selection of these objects was more implicit in nature, with no explicit AGN luminosity cutoff used.

We refer to Simmons et al. (2017) for further information on the selection and analysis of this initial 137 source sample.

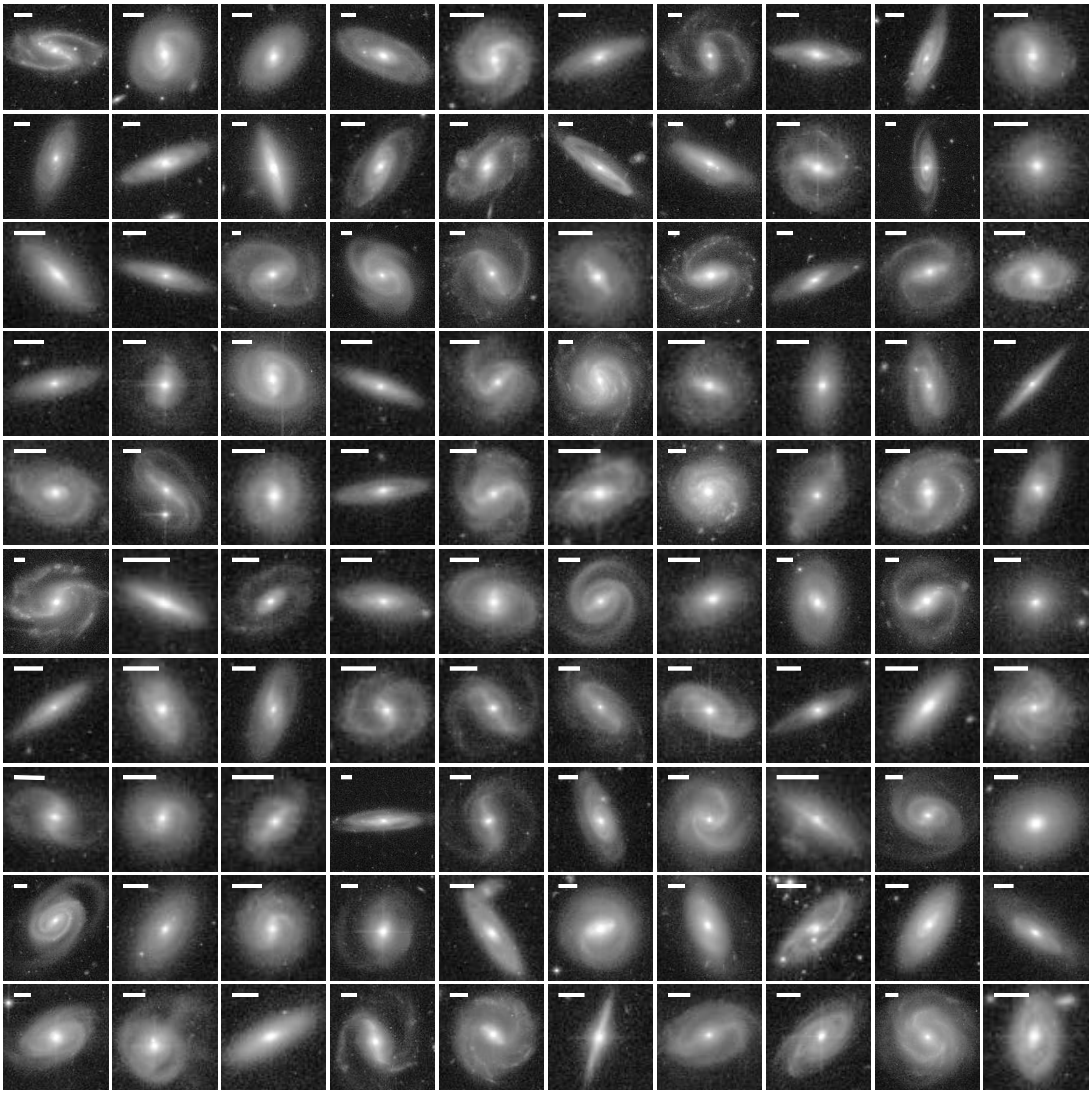

Figure 2.1 Postage stamp *HST* images of the sample of 100 disk-dominated galaxies with unobscured, luminous AGN. Sample selection is described in Chapters 2 and 2.1. Images are displayed in the order they were imaged by *HST*. Scale bars in each panel show 5". These 100 sources comprise our sample for analysis.

2.1 *HST* Snapshot Survey

All previous work that utilises parts of the Simmons et al. (2017) parent sample has been reliant upon SDSS imagery for optical morphology determination. Furthermore, apart from 2 objects with dedicated Isaac Newton Telescope (INT) imagery, all of the bulge-to-total ratio and bulge stellar mass estimates of Simmons et al. (2017) are considered conservative upper limits due to the presence of the luminous AGN. These limitations motivated a follow-up survey performed using *HST* in order to obtain much more detailed imagery.

This *HST* snapshot survey (programmme ID *HST*-GO-14606 PI: Simmons) was performed with broad band imaging in the F814W, F850LP, and F775W filters using Advanced Camera for Surveys (ACS) Wide Field Camera (WFC). *HST*'s ACS module is chosen due its very stable and extremely well-modeled point spread function (PSF), which is key for the accurate separation of host galaxy from AGN. F775W is chosen for observations of targets at $z < 0.06$, F814W for targets at $0.06 < z < 0.08$, and F850LP for targets at $z > 0.08$. This filter choice enables imaging in the reddest possible broadband rest-frame optical filter that is not significantly affected by dust, allowing for the detection of typically redder bulge emission which will be key for accurate host galaxy decomposition. 101 galaxies were imaged in total: 3 in F775W, 38 in F814W, and 60 in F850LP, and these images were reduced using the standard *HST* pipeline. These reduced images have a pixel scale of 0.05" per pixel, which corresponds to a physical pixel scale of 0.041 kpc, 0.12 kpc, and 0.19 kpc at the minimum ($z = 0.042$), median ($z = 0.129$), and maximum ($z = 0.242$) redshift of the sample respectively.

High resolution *HST* imagery enabled further confirmation of the visual classifications assigned in Simmons et al. (2017). One galaxy is excluded due to failed guide star acquisition. As such, the 100 remaining galaxies imaged by *HST* comprise our sample for analysis. Postage stamp images of these 100 galaxies are shown in Figure 2.1.

Chapter 3

Structural Decomposition

When inspecting galaxy images, previous work has pointed to the confusion that can arise in distinguishing between point sources due to an AGN, and the presence of a classical galaxy bulge (Simmons & Urry, 2008). Hence, for a quantitative and robust decomposition of galaxy morphology parametric fitting is necessary. Engaging in a parametric fitting procedure allows for both an independent assessment of host morphology, and quantitative separation between disk and bulge, providing constraints on possible bulge contribution.

3.1 Parametric fitting with `GALFIT`

We use the two-dimensional parametric image fitting program `GALFIT` (Peng et al., 2002, 2010) to simultaneously model the unresolved nucleus and extended galaxy for each of the galaxies in the sample using the *HST* imagery discussed above (see e.g. Dunlop et al., 2003, Gabor et al., 2009, Schawinski et al., 2011, 2012, Simmons et al., 2011).

Initially we make use of a batch fitting procedure to fit each source three times. In the first fit, the source is modelled with a combination of a single Sérsic profile (Sersic, 1968) and a central point source. In the second fit, the source is modelled with a combination of a single Sérsic profile, an exponential disk profile, and a central point source. In the third fit, the source is modelled with a combination

Figure 3.1 Postage stamp images of galaxy J003432.51+391836.1 as it goes through the fitting procedure. The first panel shows the galaxy as imaged by *HST* ACS WFC in the F814W filter. The second panel shows the best GALFIT residual after undergoing the batch fitting process. The third panel shows the best GALFIT residual after undergoing the final manual fitting procedure. All companion galaxies that are not included within the fit are masked so as not to contaminate the fit.

of a single Sérsic profile, a classical de Vaucouleurs (1953) bulge profile, and a central point source.

Initial parameters (magnitude, radius, axis ratio and position angle) were either drawn from the SDSS catalogue, or estimated based upon inspection of the galaxy images. The host Sérsic index is set to $n = 2.5$ and allowed to vary. This value was chosen so as to avoid favouring either an exponential disk ($n = 1$) or a classical de Vaucouleurs (1953) bulge ($n = 4$). The exponential disk and bulge profile in the second and third fits respectively are initialised in a similar way, as Sérsic components with Sérsic indices fixed to $n = 1$ and $n = 4$ respectively. The primary purpose of these initial fits are to converge on the centroid positions of each of the dominant galaxy components. During the batch fitting procedure we also fix the sky background to an independently determined value for each nearby source. Any object whose light profile is not impinging on the central galaxy is masked from the fit. In the case where nearby bright stars or companion galaxies impinge on the central galaxy, the relevant object is fit with its own component and noted as a 'companion' (classification of morphological components will be discussed further in Chapter 3.2). The primary goal of the fit is to neither over nor under subtract the galaxy's central region.

The residuals of these three initial fits are inspected for each galaxy, and the best fit is then selected to undergo a further manual fitting process. During the manual fitting process additional model components were inserted based upon iterative inspection of the fit residuals, with the same goal as outlined previously to neither over nor under subtract the galaxy's central region. In addition, great care was taken to ensure the chosen galaxy best fit contains component parameters which are physically reasonable. Additional model components could take the form of any component allowed by GALFIT, but were typically additional Sérsic components. In some cases, these Sérsic components required modification to best fit galaxy morphologies, the most prominent examples of these being modification by truncation to model a strong galactic bar, or modification by power-law rotation to model bright spiral-arms.

For illustration, Figure 3.1 shows galaxy J003432.51+391836.1 as it goes through the fitting procedure. The best model from the batch fitting procedure contains 3 components, a PSF to model the nuclear emission, a disk component with fixed Sérsic index ($n = 1$), and an additional Sérsic component with a free Sérsic index that models a small central pseudobulge. During the manual fitting process 2 additional Sérsic components are added for a total of 5 components including the PSF. One of these additional components is to model the bright spiral arms clearly visible in the batch fit residual (Figure 3.1 centre panel), and the other is to model a short central galactic bar also present in the batch fit residual. The residual from this manual fit is displayed in the right panel of Figure 3.1.

During the manual fitting process component parameters are allowed to vary in as many cases as possible. This is to ensure the fit converges to a local minima i.e. is a "stable" fit, and also to ensure the most robust and accurate component parameters are reported. In addition, the sky background is allowed to vary during this manual fitting process in order to ensure the extended regions of the galaxy are well constrained.

In order to obtain surface brightness (SB) values at the effective radius for each component each of these fits is re-run a second time. During this second fitting all parameters other than the SB remain fixed to those determined during the manual fitting procedure outlined above. For five galaxies (J090954.61+564235.3, J093545.07+320159.1, J095309.03+475113.0, J150747.63+172624.4, and

J154547.56+122201.8) only SB values for the bulge components could be recovered, and hence the additional components in these fits only have full integrated magnitudes.

Following this round of fitting, 8 galaxies are removed from the sample having been identified as having morphologies consistent with elliptical galaxies, leaving us with 92 galaxies for further analysis. Given previous work has been reliant upon SDSS imagery and visual identification, it is encouraging that our in-depth fitting shows that these previous methods are still robust enough to select small samples of disk-dominated galaxies at $\gtrsim 90\%$ confidence.

In this final sample of 92 galaxies every galaxy was fit with at least three components including the PSF, and most galaxies (>78%) are fit with at least four components including the PSF. A smaller proportion of galaxies (26%) contain five components including the PSF, and only a single galaxy in our sample is fit with six components including the PSF.

3.2 Component Classification

In order to quantify the contribution of differing components to the host galaxy luminosity (e.g. bulge contribution, pseudobulge contribution) each individual component within a given galaxy must be assigned a classification. This initial classification was carried out by a single expert classifier (MJF).

Possible initial classifications were: 'disk', 'bulge', 'spiral arms', 'bar', and 'companion'. Particular attention was paid to the final Sérsic index of a given component as well as its effective radius, with large components with low Sérsic indexes assigned 'disk' classifications, and small components with high Sérsic indexes assigned 'bulge' classifications. In order not to underestimate the bulge contribution, 'bulge' classifications are also assigned to more compact central galaxy components. At this initial stage no attempt is made to distinguish between classical bulges, and visually similar pseudobulge components. Separating these component types is discussed in Chapter 3.2.1. 'spiral arms' components were easily identified through the presence of 'spiral inner/outer radius' parameters in the final fit for that component, and 'bar' components were similarly identified by the presence of 'truncation' parameters. 'companion' galaxies were most easily identified by their significantly offset x and y coordinates relative to the PSF.

3.2.1 The Kormendy Relation

The following procedure involving the Kormendy relation is only used for further classification of 'bulge' components. Classification of 'disk', 'spiral arms', 'bar', and 'companion' components are unaffected.

When considering the classification of galaxy components a key distinction to make is that between true, classical bulge components and pseudobulge components. Pseudobulges present in galaxies as dense central components, making them visually almost indistinguishable from classical bulges. However, pseudobulges are actually far more disk-like in their structure, likely being created through secular growth processes by galaxy disks from galaxy disk material (Kormendy & Kennicutt, 2004). As these components are not created by galaxy mergers, identifying them within our sample is of paramount importance.

Follow-up classification of the compact components labelled 'bulge' in the initial classification was achieved by making use of the Kormendy relation (Hamabe & Kormendy, 1987, Kormendy, 1977). The Kormendy relation describes the relationship between effective radius and surface brightness measured at the effective radius for elliptical galaxies. Objects which lie on or above the relation are likely dispersion supported i.e. ellipticals, classical bulges. Objects which lie below the relation are likely rotation supported i.e. disks, pseudobulges. From Nigoche-Netro et al. (2008) we choose the parameters of the Kormendy relation corresponding to the magnitude range of our sample in the SDSS i and z bands, $-20.0 > M_* > -25.0$.

Figure 3.2 shows each component initially classified as 'disk' or 'bulge' in our sample of 92 disk-dominated galaxies, with their Sérsic index indicated using the colour bar. The chosen Kormendy relations for the SDSS i and z band are shown with solid black and purple lines respectively, with the shaded region indicating the 1σ confidence intervals from Nigoche-Netro et al. (2008).

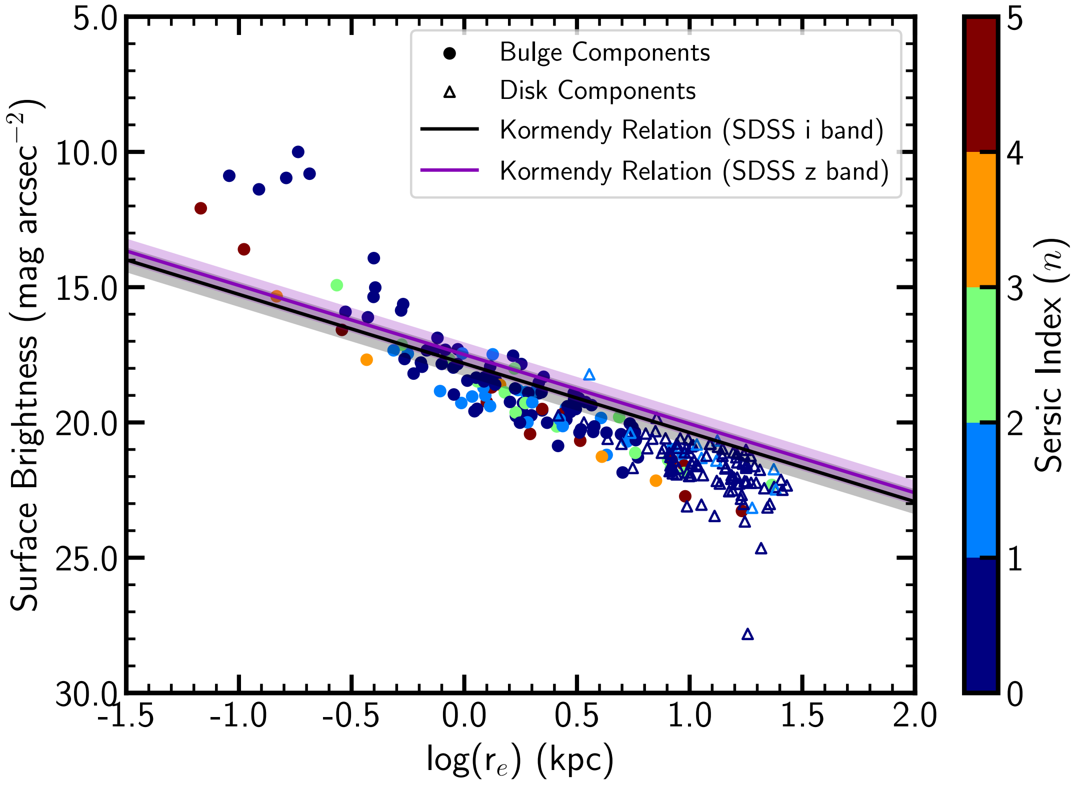

Figure 3.2 Surface Brightness at the effective radius as a function of the effective radius for each of the components initially assigned a 'disk' or 'bulge' classification in our sample for the 92 galaxies identified as disk-dominated. 'disk' components are shown with hollow triangular markers, while 'bulge' components are assigned circular markers. The Sérsic index of a given component is indicated using the colour bar. The colour bar saturates at $n = 4$ in order to aid visual interpretation, such that components with Sérsic indices $n \geq 4$ all appear in the same (reddish brown) colour. Kormendy relations for the SDSS i and z band are shown with the solid black and purple lines respectively. Shaded regions represent 1σ confidence intervals.

Any 'bulge' component which lies below the 1σ confidence interval of the SDSS i band relation (black) is designated a 'pseudobulge' as its final classification, and any 'bulge' component which lies on or above this line is considered a true classical bulge and is designated a 'bulge' as its final classification. We choose this threshold in order to minimise the chances of underestimating the contributions of classical bulges to our sample. In total we find 49 galaxies hosting a classical bulge, or $53.3 \pm 0.5\%$ of the sample.

It is clear from Figure 3.2 that the vast majority of 'bulge' and 'disk' components lie below the Kormendy relation for the SDSS i and z band. This implies most components in the sample are rotation supported structures, confirming that these galaxies are indeed overwhelmingly disk-dominated in their morphologies. In addition, we find that true bulge components within the sample are small compared to the pseudobulge and disk components, with an average effective radius of 1.33 kpc at the median redshift of our sample ($z = 0.129$).

Previous studies have often used the Sérsic index of a component in order to distinguish between classical bulge and pseudobulge, with a typical divider of $n = 2$ found to be a reliable metric for characterising a large sample (Fisher & Drory, 2008). However, Figure 3.2 highlights that the Sérsic index alone is not a reliable indicator of the true nature of a bulge-like component within our sample, and this is consistent with Gadotti (2008) who find that the use of the bulge Sérsic index is not the most robust parameter for quantitatively morphologically classifying such components. We find numerous classical bulges presenting with measured Sérsic indexes in the range $n \sim 0-1$, and conversely many pseudobulge components have Sérsic indexes $n \gtrsim 4$. This further underlines the paramount importance of utilising parametric fitting techniques to accurately decompose and classify galaxy components.

Gadotti (2008) also note that the structural parameters of bulges (and in particular bulge Sérsic index) are profoundly affected by improper modelling of luminous AGN or galactic bars. Whilst every care has been taken during our fitting procedure to accurately model the AGN through the PSF and to fit accurate galactic bar components, we recognise that our sample is somewhat extreme when compared to the general galaxy population; with small bulges in comparison to dominant disks, combined with very bright central AGN. Hence, our use of the Kormendy relation for bulge classification helps to somewhat mitigate these issues, as whilst individual Sérsic indexes may be poorly constrained, utilising both component effective radius and component surface brightness at the effective radius allows us to more accurately determine the morphological nature of a given component.

It should also be noted that due to the complexity of performing multi-component fits in `GALFIT`, it is possible that the initial classification outlined at the beginning of Chapter 3.2 has resulted in some components being incorrectly classified. This would explain why a number of 'bulge' components in Figure 3.2 have effective radii comparable to those of 'disk' components. Similarly to the issue outlined above regarding improper modelling of luminous AGN or galactic bars, our use of the Kormendy relation should help to mitigate the effects of misclassification through reliable separation of rotation and dispersion supported structures. In this way, a 'disk' component initially misclassified as a 'bulge' component should receive a final classification of 'pseudobulge' following application of the Kormendy relation. Hence, the bulge contribution of a given galaxy should not be significantly over or under estimated, and as such the effects of initial misclassification should not significantly impact the results outlined below.

Chapter 4

Additional Sample Parameters

In order to accurately determine how galaxy and black hole growth may correlate in the absence of major mergers, we require accurate estimates of additional sample parameters including luminosity ratios, galaxy stellar masses, bulge stellar masses, black hole masses, AGN luminosities, accretion rates, and Eddington ratios.

4.1 Luminosity Ratios

Having carried out the component classification detailed in Chapter 3.2 we compute AGN-to-total, bulge-to-total, and pseudobulge-to-total luminosity ratios for each galaxy in the sample.

The host galaxy luminosity is taken as the sum of the luminosity of each component used to fit the galaxy, excluding the PSF which represents the nuclear emission (as such, when computing AGN-to-total ratios we assume the PSF luminosity represents the entirety of the AGN luminosity).

The bulge and pseudobulge luminosities are taken to be the sum of the luminosity of each component used to fit the galaxy with the appropriate 'bulge' and 'pseudobulge' classification, following the application of the Kormendy relation (see Chapter 3.2.1).

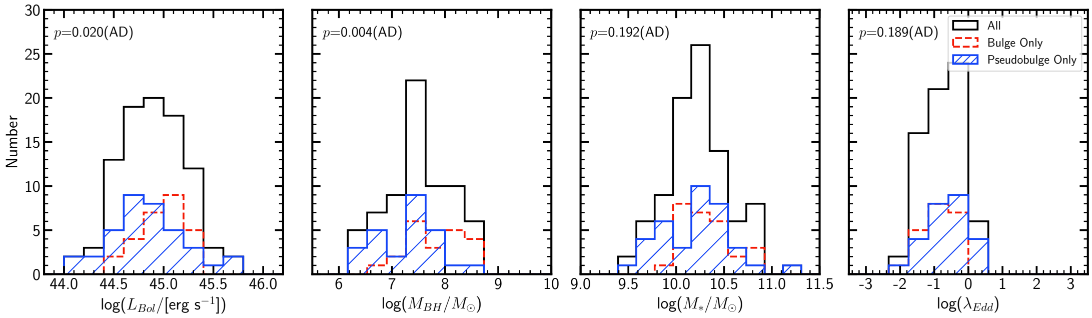

Figure 4.1 Properties of our sample: panels show distributions of bolometric luminosity, L_{Bol} (far left), black hole mass, M_{BH} (centre left), galaxy stellar mass M_* (centre right), and Eddington fraction, λ_{Edd} (far right) for the entire sample (black), for galaxies which contain only bulge components (red dashed), for galaxies which contain only pseudobulge components (blue hatched). Labels in the top left report p values for Anderson-Darling tests for statistical significance when comparing the bulge only and pseudobulge only samples. For the L_{Bol} and M_{BH} distributions we reject the null hypothesis that the bulge only and pseudobulge only samples are drawn from the same population, with $p = 0.020$ and $p = 0.004$ (Anderson-Darling test) respectively. For the distributions of M_*, and λ_{Edd} these two samples are more similar and the null hypothesis cannot be confidently ruled out.

Table 4.1 Tests for statistical significance performed on the bulge only and pseudobulge only distributions from Figure 4.1. p values are reported for both Kolmogorov-Smirnov (KS) and Anderson-Darling (AD) frameworks. For the M_*, and λ_{Edd} distributions we cannot confidently rule out the null hypothesis. For the L_{Bol} and M_{BH} distributions we reject the null hypothesis, and find AD statistics of 2.97 and 4.76, indicating statistically significant differences in these populations to 2.3σ and 2.9σ respectively.

	p value (KS)	p value (AD)
AGN Bolometric Luminosity (L_{Bol})	0.016	0.020
Black Hole Mass (M_{BH})	0.012	0.004
Galaxy Stellar Mass (M_*)	0.099	0.192
Eddington Fraction (λ_{Edd})	0.384	0.189

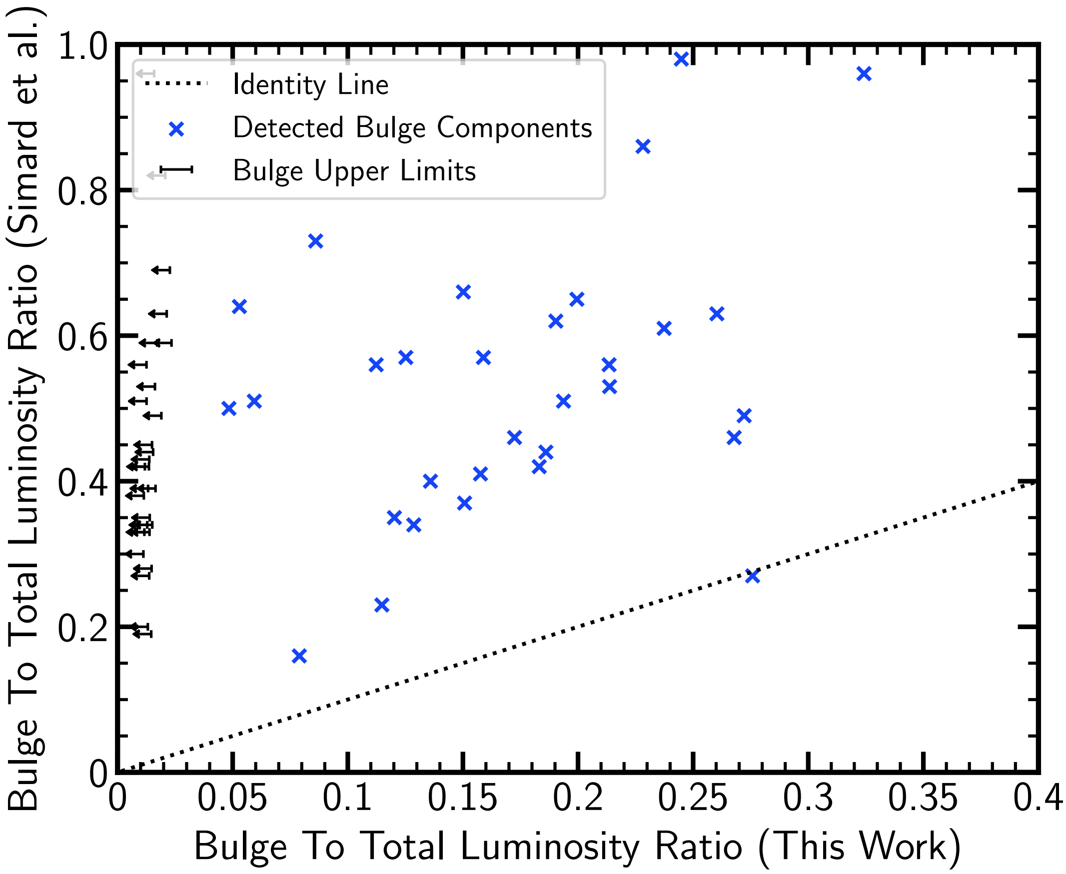

Figure 4.2 Recovered bulge-to-total luminosity ratios for the 59 galaxies from our disk-dominated sample that also appear in the catalogue of Simard et al. (2011). Galaxies from our sample with detected bulge components are shown with blue crosses, whilst galaxies with no detected bulge components have the upper limits on their bulge-to-total ratios indicated with black arrows. In order to aid visual interpretation these limits are given an additional +0.01 shift along the x axis, and we include the Identity Line ($y = x$) as a black dotted line. We find that >98% of these galaxies have reported bulge-to-total ratios in Simard et al. (2011) that are higher than those found by this work. Such findings clearly show the magnitude to which bulge contribution to galaxy luminosity can be artificially inflated if a bright AGN is not accounted for during bulge-disk decomposition.

As mentioned in Chapter 3.2.1, it is possible that some disk components have been misclassified as pseudobulges. Whilst this might artificially inflate the pseudobulge-to-total luminosity ratios for individual sources, the effect should not be statistically significant when we consider the sample as a whole. Furthermore, this work is primarily focused on the effects of merger vs. non-merger driven galaxy evolution, and hence the primary concern is the separation of dispersion supported classical bulge components from rotation supported disk and pseudobulge components.

The AGN-to-total ratio for the sample lies between $0.003 < \mathrm{AGN/Tot} < 1.6$, with a mean value of 0.2 ± 0.2, and a median value of 0.19 ± 0.03. This further indicates the highly luminous nature of the AGN in the sample, and the importance of robustly constraining the PSF when engaging in structural decomposition of AGN host galaxies.

For galaxies with detected bulges, the bulge-to-total ratios lie between 0.04 $< (\mathrm{B/Tot}) < 0.52$, with a mean value of 0.2 ± 0.1 and a median value of 0.18 ± 0.02. When we include galaxies with no detected bulge component the mean and median bulge-to-total ratios for the sample drop to 0.1 ± 0.1 and 0.06 ± 0.03 respectively.

Simard et al. (2011) carried out bulge-disk structural decomposition of 1.12 million galaxies in the SDSS DR7 Legacy area, determining best-fit models and structural parameters for each. Simmons et al. (2017) take the r-band bulge-to-total ratio of the best-fit model as an upper limit to the true bulge-to-total ratio of these AGN host galaxies. The upper bulge-to-total limits of the 90 galaxies in their sample which were included in Simard et al. (2011) lie between $0.13 \leq (\mathrm{B/Tot}) \leq 1.0$, with a mean value of 0.5. In addition, Simmons et al. (2017) constrain 2 of the sources imaged with the INT to have bulge-to-total ratios of 0.3 ± 0.2 and 0.47 ± 0.2.

We similarly match our galaxy catalogue to Simard et al. (2011), and find 59 galaxies which appear in both catalogues. Following Simmons et al. (2017), we find bulge to total ratios in the range $0.16 \leq (\mathrm{B/Tot}) \leq 0.98$, with a mean value of 0.5. Figure 4.2 shows a comparison of the recovered bulge-to-total ratios of our galaxies versus those recovered by Simard et al. (2011). Galaxies in our sample with detected bulges are shown with blue crosses, whilst upper limits on bulge-to-total ratios for those galaxies with no detected bulge component are shown with black arrows, which have been given a +0.01 shift in the x to aid visual interpretation (the methodology for calculating these upper limits is discussed further below in this chapter).

As such, our mean bulge-to-total ratio for the entire sample (including galaxies with no detected bulge component) lies below even the smallest upper bulge-to-total limit of the Simard et al. (2011) galaxies. When we consider only those galaxies with detected bulges, the mean bulge-to-total ratio for our sample lies below both the mean bulge-to-total ratio from the Simard et al. (2011) sample, and each of the individually constrained bulge-to-total ratios from Simmons et al. (2017), strongly indicating that the overall bulge contribution to this sample is small, despite $> 50\%$ of the galaxies in the sample containing a classical bulge component (see Chapter 3.2.1). Such findings are further reinforced when considering the Kormendy relation (See Figure 3.2 and Chapter 3.2.1), where we find that the vast majority of components lie in the region typically populated with rotation supported objects i.e. disks and pseudobulges, with only a small fraction of objects considered true bulges.

For galaxies with detected pseudobulges, the pseudobulge-to-total ratio ranges from $0.03 < \mathrm{Pseudo/Tot} < 0.96$, with a mean value of 0.3 ± 0.3, and a median value of 0.2 ± 0.3. When we include galaxies with no detected pseudobulge component the mean and median pseudobulge-to-total ratios for the sample drop to 0.2 ± 0.2 and 0.09 ± 0.03 respectively. As such, we find in either case that the mean pseudobulge-to-total ratios are comparable, if not larger than the the mean bulge-to-total ratios reported above, indicating the increased prevalence of pseudobulge components within the sample. Indeed, when we consider the subset of galaxies ($23.9 \pm 0.2\%$) in our sample which contain both pseudobulges and classical bulges, we find mean pseudobulge-to-total and bulge-to-total ratios of 0.3 ± 0.2 and 0.2 ± 0.1 respectively, further reinforcing our findings outlined above.

As such, we can say with confidence that even when considering compact central components in our galaxies, the majority of components are rotation dominated in nature. Such findings further reinforce the importance of using robust classification frameworks to differentiate these visually similar but dynamically different components. Furthermore, Figure 4.2 clearly demonstrates the effect of not taking into account a bright AGN when performing galaxy bulge-disk decomposition, with the bulge contribution to galaxy luminosity significantly artificially inflated. Considering only the galaxies with detected bulges we find that the Simard et al. (2011) bulge-to-total ratios are larger than those recovered in this work by factor of $\sim$3.75 on average, and we find some bulge-to-total ratios are larger by a factor of $\geq$10.

When considering the highly luminous nature of our AGN in conjunction with the findings of Chapter 3.2.1 that the classical bulge components in this sample are typically very small (mean effective radius of 1.33 kpc at the median redshift of our sample $z = 0.129$) it is a possibility that some true bulge components have not been recovered due to the presence of the luminous AGN. In order to minimise the chances of underestimating the contributions of classical bulges to our sample, we carry out the following procedure on all galaxies regardless of whether or not they contain a detected bulge component.

The full width at half-maximum (FWHM) of *HST* ACS is 2.5 pixels. As such, the largest bulge component that could be 'hidden' underneath a PSF in our sample would have effective radius of 1.25 pixels, subtending an angle of 0.0625" on the sky. We compute the size of such a bulge in kpc for each of our galaxies, and then use the Kormendy relation for the SDSS z band (see Figure 3.2) to obtain an estimate of the surface brightness at the effective radius for each of these objects. We choose the z band relation as this gives us the brightest possible value of surface brightness and will prevent the contribution from any 'hidden' bulge component being underestimated. We use this surface brightness to calculate the luminosity of this extra 'hidden' bulge component.

For galaxies with no detected bulge component, the luminosity ratio of this 'hidden' bulge to the total host galaxy luminosity is considered an upper limit of the bulge-to-total luminosity ratio for that object. We find these upper limits lie between $0.001 < (\mathrm{B/Tot})_{\mathrm{max}} < 0.013$, with a mean value of 0.006 ± 0.004. For galaxies with a detected bulge component we utilise this extra luminosity in conjunction with the already calculated errors on the luminosity of the detected bulge components to inform the upper uncertainties on our bulge-to-total ratios for these galaxies.

4.2 Galaxy and Bulge Stellar Masses

To calculate stellar masses we follow a similar methodology to that laid out in Simmons et al. (2017), using the well-studied relation between stellar mass, absolute galaxy r-band magnitude, and $u-r$ galaxy colour (corrected for Galactic extinction; Schlegel et al., 1998) outlined in Baldry et al. (2006). To obtain photometry for our sample we perform a positional match to SDSS DR16 (Ahumada et al., 2020). For one galaxy (J011929.06-000839.5) no photometric data is available in DR16, and so we use photometry from SDSS DR9 (Ahn et al., 2012). In order to better remove the AGN contribution to galaxy luminosity, we correct the SDSS u and r band magnitudes for PSF contribution by multiplying the flux from the SDSS `modelMag` by the host-to-total luminosity ratio computed using our fits from `GALFIT`. Here we take the host galaxy luminosity as the sum of each galaxy component excluding the PSF. The total galaxy luminosity is the sum of each galaxy component including the PSF.

We recover stellar masses which range from $2.8\times10^{9}\mathrm{M}_{\odot} < \mathrm{M}_{*} < 8.4\times10^{10}\mathrm{M}_{\odot}$. The median stellar mass is $1.7\times10^{10}\mathrm{M}_{\odot}$. Each individual mass is taken to have an uncertainty of 0.3 dex from the scatter in the colour-luminosity relation. The centre right panel of Figure 4.1 displays the galaxy stellar mass distribution for our sample. The stellar mass distribution for the entire sample is shown in black. The stellar mass distribution for objects which have only a bulge contribution (bulge-to-total $\neq 0$, pseudobulge-to-total $= 0$) is shown in dashed red, and the the stellar mass distribution for objects which have only a pseudobulge contribution (bulge-to-total $= 0$, pseudobulge-to-total $\neq 0$) is shown in hatched blue.

Table 4.1 summarises Kolomogrov-Smirnov (KS) and Anderson-Darling (AD) Tests for statistical significance for the sample properties displayed in Figure 4.1. We find p values of $p = 0.099$ (KS) and $p = 0.192$ (AD) when comparing the bulge-only and pseudobulge-only samples likely indicating we cannot rule out the null hypothesis. We note that the p value for the KS test is noticeably lower than that reported for the AD test, and upon inspecting Figure 4.1 we find that whilst at high and median masses the distribution of the bulge-only and pseudobulge-only samples are very comparable, the bulge-only sample seems to lack the same low mass tail displayed by the pseudobulge-only sample, dropping off rapidly at $\sim 10^{10}\mathrm{M}_{\odot}$. This could indicate that the galaxies in our sample which host bulges tend to have stellar masses above a certain mass threshold, with few galaxies at low stellar mass. These findings are consistent with Skibba et al. (2012), who find a strong correlation between bulge strength and galaxy stellar mass in their sample of $\sim$ 16,000 disk galaxies at $z < 0.06$. Most strikingly, the transition from disk-dominated to bulge-dominated for this correlation appears at $\mathrm{M}_{*} \approx 2 \times 10^{10}\mathrm{M}_{\odot}$, very close to the threshold in our sample below which galaxies hosting classical bulges are mostly absent. Such findings could indicate that these bulge-only galaxies are present in different environments to those of the pseudobulge only sample. Higher density environments might allow for better accretion of cold molecular gas and lead to increased star formation, as well as increasing the likelihood of galaxy mergers (major or minor) explaining why these objects which host bulges also seem to possess stellar masses above a given threshold. This is consistent with the findings of Skibba et al. (2012) who report their bulge-dominated disk galaxies reside in denser environments. Further work to investigate the star formation rates of these objects, as well as their gas supply and local environment might shed further light on the extent to which these are affecting long term star formation in our bulge-only sample. We highlight here however that, as mentioned previously, when we also consider the p value from the AD test we find that the bulge-only and pseudobulge-only samples are highly comparable.

We note that these stellar masses are significantly lower than those reported in Simmons et al. (2017) of $8 \times 10^{9}\mathrm{M}_{\odot} < \mathrm{M}_{*} < 2 \times 10^{11}\mathrm{M}_{\odot}$, with a mean galaxy stellar mass of $4 \times 10^{10}\mathrm{M}_{\odot}$. We attribute these differences primarily to changes in the SDSS pipeline from DR8 to DR16, which have particular effect on recovering galaxy magnitudes in the u-band.

Having calculated luminosity ratios above (see Chapter 4.1) we use these in conjunction with the calculated stellar masses in order to obtain estimates of bulge stellar masses for each of our galaxies. These correspond to bulge stellar masses (for those galaxies with detected bulges) in the range $3.9 \times 10^{8}\mathrm{M}_{\odot} < \mathrm{M}_{\mathrm{Bulge}} < 1.8 \times 10^{10}\mathrm{M}_{\odot}$, with a mean bulge stellar mass of $3 \times 10^{9}\mathrm{M}_{\odot}$.

When we consider the upper limits on the bulge-to-total ratios for those galaxies with no detected bulge contribution (see Chapter 4.1) we find they correspond to bulge stellar masses in the range $1.7 \times 10^7 M_\odot < M_{\text{Bulge Max}} < 4.4 \times 10^8 M_\odot$, with a mean bulge mass of $7.4 \times 10^7 M_\odot$.

4.3 Black Hole Masses

Simmons et al. (2017) use the relation of Greene & Ho (2005) (subsequently re-calibrated by Shen et al., 2011) to obtain black hole masses from the established relationship between black hole mass and the FWHM and luminosity in the broad Hα line. This relation is chosen to avoid contamination of the spectra by the host galaxy, and also as Hα was available for all spectra in this sample. A bootstrap method was used by Simmons et al. (2017) in order to estimate the uncertainties on these black hole masses. As such, we recover black hole mass estimates for 68 of the galaxies in our sample. We refer to Simmons et al. (2017) for further information regarding the calculation of black hole masses.

The black hole masses for the sample range from $1.8 \times 10^6 M_\odot < M_{BH} < 4.8 \times 10^8 M_\odot$. The median mass is $3.0 \times 10^7 M_\odot$.

The centre left panel of Figure 4.1 shows the black hole mass distribution for our sample. There is strong indication that the bulge only galaxies within our sample lie at the higher mass end, with median black hole masses of $7.3 \times 10^7 M_\odot$ compared to a median mass of $2.4 \times 10^7 M_\odot$ for the pseudobulge only population.

The p values of $p = 0.012$ (KS) and $p = 0.004$ (AD) strongly indicate that the null hypothesis can be ruled out, and we find when consulting the AD results that the bulge only and pseudobulge only populations differ to a statistical significance of 2.9σ. These findings suggest that, within our sample, galaxies which host bulges show indications of hosting more overly massive black holes in comparison to those galaxies which do not host any bulge component.

We do note however that these black hole masses are of the same order of magnitude, indicating that whilst merger events may result in increased black hole mass we still question the extent to which they are the dominant mechanism facilitating this. Recent simulation work from Martin et al. (2018) and McAlpine et al. (2020) suggest mergers play little role in black hole growth in the long term, and this point is further highlighted when we consider those galaxies in the sample which host neither a pseudobulge nor a classical bulge which present with a median black hole mass of $2.9 \times 10^7 M_{\odot}$. Such black hole masses are highly comparable to the overall sample and easily breach $10^7 M_{\odot}$, some of the highest masses for such galaxies reported in the literature, challenging previous notions that galaxies which are truly bulgeless (no pseudobulge or bulge contribution) should struggle to grow their black holes above $\sim 10^{5-6} M_{\odot}$ (Satyapal et al., 2008, 2009, Secrest et al., 2012). These findings are in agreement with more recent literature that has also confirmed black holes grown to supermassive size through secular processes, independent of major mergers (Bohn et al., 2020, 2022).

As such, whilst we find evidence that galaxies that may have been involved in past mergers experience enhanced black hole growth, our findings still question the notion that galaxy mergers are the primary driver of this growth in the long term, with ample evidence of galaxies which are merger free growing their black holes to significant and comparable mass in the local Universe. We note here however that the selection techniques used to compose this sample preferentially select the most luminous AGN, which may be more likely to have higher black hole masses due to their rapid observable growth. As such, we find it plausible that the truly bulgeless galaxies in our sample with massive black holes $\geq 10^7 M_{\odot}$ represent the extreme tail of a distribution of black holes fuelled by purely secular growth. This would suggest that whilst it is possible to grow black holes to masses in excess of $\sim 10^{5-6} M_{\odot}$ through purely secular processes, such black holes are not necessarily representative of the global black hole population fuelled by these processes alone. Further study of more moderate luminosity AGN hosted in disk-dominated galaxies would aid in better understanding the overall distribution of black hole masses in these systems, and the frequency at which such black holes grow to $\geq 10^7 M_{\odot}$.

4.4 AGN Luminosities, Accretion, and Eddington Ratios

Bolometric AGN luminosities, the luminosity of the AGN when integrated across the entire electromagnetic spectrum, L_{Bol}, for the sample are estimated following

Simmons et al. (2017) utilising the *Wide-field Infrared Survey Explorer* (*WISE*) W3 band centred at 12μm. We choose a bolometric correction factor of ≈ 8 from Richards et al. (2006), which does not depend significantly on wavelength in the infrared (see their Figure 12).

The AGN bolometric luminosities for the sample range from 1.1×10^{44}ergs^{-1} $\leq \mathrm{L}_{\mathrm{Bol}} \leq 5.5 \times 10^{45}$ergs^{-1}. The median luminosity is 7.7×10^{44}ergs^{-1}.

The far left panel of Figure 4.1 shows the AGN bolometric luminosity distribution for our sample. We find p values of $p = 0.016$ (KS) and $p = 0.020$ (AD) when comparing the bulge-only and pseudobulge-only samples (Table 4.1), with the bulge-only sample shifted slightly towards higher luminosities. These p values indicate the null hypothesis can likely be ruled out for these sub-samples, and consulting the results of the AD test we find these populations differ to a statistical significance of 2.3σ. This finding suggests that, within our sample, galaxies which host bulges are also hosting more luminous AGN.

Previous observational studies have found luminous quasars are seemingly preferentially hosted in ongoing mergers (Glikman et al., 2015, Trakhtenbrot et al., 2017, Urrutia et al., 2008, Volonteri & Rees, 2006), and simulations have revealed mergers may increase the rate of luminous AGN (McAlpine et al., 2020), findings which may support the increased incidence of luminous AGN in the galaxies hosting bulges in our sample. Furthermore, when we consider these results in conjunction with our findings in Chapters 4.2 and 4.3 it is possible that these AGN display increased luminosity due to their higher mass black holes and potentially more dense environments.

However, the above referenced works concern galaxies engaged in ongoing mergers, whilst the galaxies in our sample have been specifically selected due to a lack of indication of them engaging in a major merger event since $z \sim 2$. Given that typical AGN duty cycles are measured on the order of 10^{5-6} yr (Keel et al., 2012, Schawinski et al., 2015), it seems unlikely that merger events in the distant past are influencing their AGN luminosities in the present. Furthermore, studies such as Woo & Urry (2002) find no indication of significant correlation between black hole mass and luminosity, indicating that the higher black hole masses of the bulge only sample should not also be responsible for their increased AGN luminosities.

Our findings may be explained by considering our results in Chapters 4.2 and 4.3 on a broader scale in that they may indicate that the galaxies within our sample reside in denser environments. Such environmental density might produce the effect of simultaneously facilitating more galaxy mergers resulting in an increased proportion of bulge components, and allowing for increased inflow of cool molecular gas allowing for enhanced star formation and increased total galaxy stellar mass. These two processes could be working in tandem to funnel more gas to the galactic centre resulting in an AGN which is more luminous and more massive. However, we do point to studies such as Smethurst et al. (2019) who make the argument that the unpredictable gas inflow geometry of merger driven fuelling should have the effect of spinning down any given black hole, resulting in lower radiative efficiency and more gas mass lost to outflows. These outcomes would have the combined effect of both limiting the gas available to grow a black hole, as well as reduce its bolometric luminosity.

The AGN bolometric luminosity is related to its mass accretion rate, $\dot{m}$ through a simple matter to energy conversion shown in Equation 4.1, where $\eta = 0.15$ (Elvis et al., 2002).

$$\dot{m} = \frac{\mathrm{L_{Bol}}}{\eta c^2} \tag{4.1}$$

Black hole masses are also used to calculate the luminosities expected if each AGN were accreting at its Eddington limit, $\mathrm{L_{Edd}}$. We use this to compute the Eddington fraction (Equation 4.2) to measure the fractional growth rate of the black hole relative to the maximum rate it is capable of sustaining.

$$\lambda_{\mathrm{Edd}} \equiv \frac{\mathrm{L_{Bol}}}{\mathrm{L_{Edd}}} \tag{4.2}$$

The far right panel of Figure 4.1 shows the Eddington fraction distribution for our sample. We find p values of $p = 0.384$ (KS) and $p = 0.189$ (AD) when comparing bulge-only and pseudobulge-only samples for Eddington fraction (Table 4.1), indicating we cannot rule out the null hypothesis. This finding suggests that, within our sample, galaxies which host bulges do not have a statistically significantly higher fractional growth rate in comparison to those which have no bulge component.

This is further support for the notion outlined above that whilst galaxy mergers might enhance black hole growth, merger events are not the dominant process facilitating it in this sample. Such highly comparable Eddington fractions imply that the dominant pathways fuelling black hole growth for both the bulge-only and pseudobulge-only subsamples are also comparable, and hints towards a more fundamental process common to every galaxy in our sample as the dominant pathway for facilitating black hole growth in the long term. As mentioned previously, this view is consistent with simulation work from McAlpine et al. (2020) and Martin et al. (2018) who suggest that mergers (major or minor) contribute as little as $\sim 35\%$ of black hole growth since $z \sim 3$.

Chapter 5

Bar Fraction

It has been proposed in the literature that galactic bars might be a crucial secular mechanism for black hole feeding by transporting gas to the central AGN (Ann & Thakur, 2005, Athanassoula, 2003, Friedli & Benz, 1993). Currently the literature is not in good agreement on relationships between AGN and galactic bars. Many studies find no correlation between AGN and bars (Cheung et al., 2015, Goulding et al., 2017, Lee et al., 2012, Martini et al., 2003, Oh et al., 2012), whilst others find that bars may be preferentially hosted in active galaxies with an overall incidence increase of $\sim 20\%$ (Knapen et al., 2000, Laine et al., 2002, Laurikainen et al., 2004). Galloway et al. (2015) note that whilst there is a higher probability of a galaxy hosting an AGN to also host a bar, they find no link between bars and the quantity or efficiency of AGN fuelling, indicating that whilst bars may trigger AGN they have little further effect once the AGN is established. Despite this, recent work by Smethurst et al. (2019) has shown that morphological features including galactic bars can theoretically match the required mean mass inflow rates for powering disk-dominated AGN, and as such, investigating the bar fraction of our sample in detail could provide crucial information about the role of bars in fuelling black hole growth.

Within the sample there are 23 galaxies that have been fit with a component modelling a galactic bar, representing $25.0 \pm 0.3\%$ of our galaxies. This fraction is consistent with previous literature including Masters et al. (2011) who found that around $29.4 \pm 0.5\%$ of disk galaxies host a large scale galactic bar at redshift

$0.01 < z < 0.06$ when imaged in the optical. Of the 23 galaxies hosting bars, 6 are completely bulgeless (no pseudobulge or classical bulge contribution), 10 host only a pseudobulge, 5 host only a classical bulge, and 2 host both a classical bulge and a pseudobulge.

The AGN bolometric luminosities for the barred galaxies range from $3.6 \times 10^{44}\mathrm{ergs}^{-1} \leq \mathrm{L_{Bol}} \leq 4.6 \times 10^{45}\mathrm{ergs}^{-1}$, with a median bolometric luminosity of $7.8 \times 10^{44}\mathrm{ergs}^{-1}$, this is in good agreement with the luminosity range of our overall sample (see Chapter 4.4), and upon performing tests for statistical significance we find p values of $p = 0.801$ (KS) and $p > 0.25$ (AD) indicating that the null hypothesis cannot be ruled out.

Black hole mass estimates are available for 18 of the barred galaxies within the sample. The masses range from $2.0 \times 10^{6}\mathrm{M}_{\odot} \leq \mathrm{M_{BH}} \leq 1.8 \times 10^{8}\mathrm{M}_{\odot}$, with a median mass of $2.9 \times 10^{7}\mathrm{M}_{\odot}$. Similarly to the AGN bolometric luminosity, the black hole masses are in very good agreement with the overall sample and upon performing tests for statistical significance we find p values of $p = 0.135$ (KS) and $p > 0.25$ (AD), also indicating that the null hypothesis cannot be ruled out.

These findings suggest that the barred galaxies within our sample are hosting neither AGN that are overly luminous, nor black holes which are overly massive when compared to our overall sample of disk galaxies.

If bars are the primary fuelling mechanism for black hole growth in the merger free regime, we might expect that AGN hosted in barred galaxies would be more luminous and have larger black hole masses when compared to unbarred galaxies. This is especially relevant when we consider that galactic bars are thought to be long-lived morphological features, and so any additional black hole growth they facilitate in the long term should be reflected in measured black hole masses in the local Universe. The fact that our findings show no tendency for overly massive black holes implies bars are simply one element of the overall picture, with some other mechanism common to all galaxies in our sample providing the majority of the fuel for black hole growth. Such findings are consistent with Galloway et al. (2015), who present a scenario wherein bar-driven fuelling contributes some fraction of the fuel for growing black holes, whilst some other processes must also contribute to black hole accretion disk fuelling through angular momentum transfer at smaller radii. This scenario is also consistent with simulations that show multiple large-scale mechanisms including galactic bars can be responsible for transporting gas to the scales required for AGN fuelling (Hopkins & Quataert, 2010). This suggests that the presence of a bar is not a requirement to grow black holes to supermassive size in the local Universe in the absence of major mergers.

Chapter 6

Galaxy-Black Hole Mass Relations

Firstly we follow Simmons et al. (2017) and investigate the relationship between black hole mass and the stellar mass attributed to the bulge. We highlight again here that the black hole-bulge relations of Simmons et al. (2017) were constrained only to a very limited extent, as $\sim 98\%$ of their bulge masses were considered upper limits. The structural decomposition completed in this work allows us to assign more accurate bulge mass estimates (see Chapter 4.2) to a significant proportion of our sample. We use a Bayesian method to fit a linear regression model to the 68 sources in our sample for which we have black hole mass estimates. This approach includes two-dimensional uncertainties. The results are displayed in the left panel of Figure 6.1. We perform two fits to our data, one where we fit only to the bulge masses of galaxies which have detected bulge components (solid black line), and one where we incorporate the upper limits on bulge masses for those galaxies which have no detected bulge component into a censored fit (dotted black line). Considering the fit to galaxies only with detected bulge components, we find a Spearman correlation coefficient of 0.35, and a Pearson correlation coefficient of 0.37 indicating some correlation, albeit with significant scatter. When we include the upper limits on bulge masses for those galaxies with no detected bulge component we find a Spearman correlation coefficient of

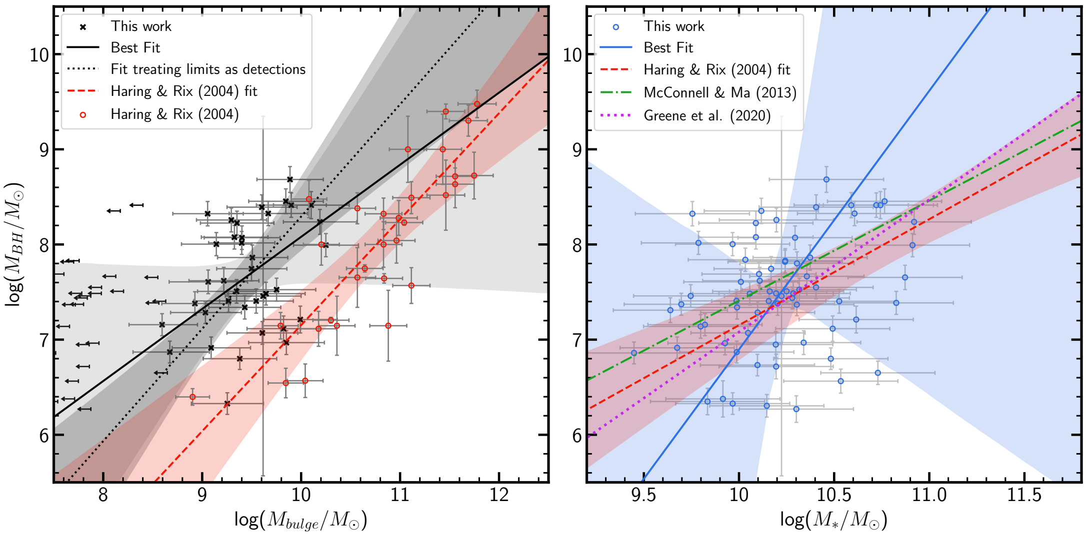

Figure 6.1 **Left Panel: Black hole-bulge relations.** Black hole mass versus bulge stellar mass. Black crosses indicate bulge masses for galaxies with detected bulge components. Arrows indicate upper limits on bulge masses for galaxies with no detected bulge component (method for calculating upper limits is given in Chapter 4.2). The best fit to galaxies with detected bulges only is shown with a solid black line. The best fit incorporating the upper limits into a censored fit is shown with a dotted line. Red open circles show early-type galaxies used to compute a canonical bulge-black hole relation (Häring & Rix, 2004); the same fitting method is applied to these data, and the best fit is indicated by the red dashed line. Shaded regions indicate 3σ confidence intervals. **Right Panel: Black hole-galaxy relations.** Black hole mass versus total stellar mass. Open blue circles show the stellar masses for our galaxies, the best fit to these is shown in the solid blue line. The relation for early-type galaxies (Häring & Rix, 2004) is again shown with the red dashed line, unchanged from the left panel. Shaded regions represent 3σ confidence intervals. We also include relations for bulge-dominated early-type galaxies from McConnell & Ma (2013) (green dot dashed) and Greene et al. (2020) (purple dotted) for further comparison. We find some evidence of a correlation between black hole mass and bulge mass, which is strengthened when incorporating the upper limits into the censored fit. However, both of these correlations are fairly inconsistent with the relation between black hole mass and bulge mass for early-type galaxies (left panel) and are significantly weaker. The fitted relation between black hole mass and total stellar mass (right panel) shows evidence of a correlation of comparable strength to that between black hole mass and bulge mass for our sample, and the fitted relation is also somewhat consistent to those of early-type galaxies, though only to within $\sim 3\sigma$, and with a large degree of scatter.

0.41, and a Pearson correlation coefficient of 0.44. Hence, in both cases we find evidence for some correlation between black hole mass and bulge mass for our sample, and this correlation is strengthened when including the upper limits on bulge mass for the sample into a censored fit.

Following Simmons et al. (2017) and for comparison, we adopt a similar procedure for a sample of early-type galaxies from Häring & Rix (2004). These galaxies have morphologies indicating a history which includes major mergers. The fitted relation for the Häring & Rix (2004) sample (red dashed line) is somewhat inconsistent with both fitted relations to our sample, and is significantly more strongly correlated, with Spearman and Pearson correlation coefficients of 0.82 and 0.83 respectively. As such, we can conclude that while there is some correlation between black holes and bulges in our disk-dominated sample, there is much stronger correlation between these two galaxy properties in bulge-dominated galaxies with rich merger histories.

The fact that the correlation is so much stronger for bulge-dominated galaxies and present but highly scattered for disk-dominated galaxies is interesting. Such findings could imply that processes which grow both bulges and black holes, such as major galaxy mergers, are the dominant co-evolutionary pathways in these early-type galaxies, and these pathways regulate such growth much more rigidly. This might explain why the early-type galaxies considered here present with bulge masses that appear to have grown in lockstep with their black holes. Disk-dominated galaxies on the other hand are engaged in these processes significantly less often, as evidenced by their lack of strong bulge components, and this may result in a more stochastic co-evolutionary history which is reflected in their highly varied bulge masses for a given black hole mass.

Previous pathways for merger driven black hole galaxy co-evolution require by design that any observed black hole-galaxy co-evolution must be driven by merger events large enough to create appreciable bulge components. As such, the fact that there is weaker correlation between bulge stellar mass and black hole mass in our sample which has been specifically selected to lack bulges might be seen as unsurprising. However, if these merger driven pathways are indeed the primary mechanisms for black hole-galaxy co-evolution, then we would also expect the black holes of our bulgeless galaxies to be undermassive, especially in comparison to those from Häring & Rix (2004) with rich merger histories. This is clearly not the case.

In Chapter 4.3 we find that the black hole masses of the truly bulgeless galaxies (those with no bulge or pseudobulge component) lie extremely close to our parent sample distribution of disk-dominated galaxies, indicating that black holes in truly merger-free systems can still grow to considerable mass. This point is further emphasised when we consider that the most massive black holes in our disk-dominated sample are of comparable mass to all but the most massive black holes (of $\sim 10^9$ $M_\odot$) in the bulge-dominated comparison sample of Häring & Rix (2004).

Furthermore, in the left panel of Figure 6.1 we see that, when we consider the galaxies with detected bulges, $\gtrsim$ 97% of them lie above the correlation for bulge-dominated galaxies, and $\gtrsim$ 90% lie above the 3σ uncertainty region for that correlation. Even when we consider the upper limits on bulge mass for the truly bulgeless galaxies in our sample, those for which no bulge component could be detected or fit in `GALFIT` we find each of them lie above both the fitted relation of Häring & Rix (2004), and the 3σ uncertainty region, and with a black hole mass distribution that is consistent in breadth with both the galaxies in our sample with detected bulges, and the majority of the galaxies in Häring & Rix (2004). These findings are clearly indicative of considerably higher black hole masses in our sample than those predicted by a bulge-black hole relation, even when we consider extremely generous upper limits on the bulge stellar masses, consistent with Simmons et al. (2017).

We note here that any analysis we have carried out in Chapter 6 thus far explicitly assumes that any detected bulge component in our disk-dominated sample has been formed and grown exclusively by merger-driven processes. However, recent observational work has suggested that classical bulges may grow and even form through processes other than major galaxy mergers.

Guo et al. (2020) find evidence that short, subkiloparsec radius bars form morphological components that bear many of the characteristics of classical bulges when they are destroyed, potentially allowing for a new channel of bulge formation in the absence of mergers. Furthermore, recent work suggests that disk galaxy bulges could form from so-called "red nuggets" (Damjanov et al., 2009). These objects present as ultra-compact spheroids at high redshift, with half light radii typically on the order of ~ 1 kpc. de la Rosa et al. (2016) confirm that compact core components of present day galaxies ($z \sim 0.1$) are structurally similar to red nuggets observed at $z \sim 1.5$, and that these components are not exclusive to massive elliptical galaxies. Such findings imply these objects could become the cores of modern day disk galaxies, a scenario also proposed by Costantin et al. (2020). This model is supported by the simulation work of Zolotov et al. (2015) and Tacchella et al. (2016), who both find evidence that extended star-forming disks develop around red nuggets after compaction. Such works suggest that very compact bulge components at the cores of disk galaxies could in fact form purely secularly, without the need for major galaxy mergers. When we consider our findings in Chapter 3.2.1 that the average classical bulge component in our sample is small, with average effective radius of 1.33 kpc at $z = 0.129$, it is perhaps possible that these bulge components (or the smallest among them) were once red nuggets at high redshift, with the disk-dominated morphology we view today subsequently forming around them. We note that this proposed formation pathway is difficult to prove without follow-up observations to investigate and constrain the dynamical properties of these small bulges.

In addition to these proposed pathways for merger free bulge formation there is a growing body of work pointing towards merger-free pathways for bulge growth. Bell et al. (2017) investigate galaxy stellar haloes in order to explore galactic merger histories and find that bulges in nearby Milky Way-like galaxies have higher than expected masses if mergers were the dominant growth mechanism for classical bulges or pseudobulges. Furthermore, Park et al. (2019) and Wang et al. (2019) both emphasise the importance of disk star migration in disk-dominated galaxies. Stars with orbits aligned with the galactic disk continuously migrate towards the galactic centre, without the need of merger-driven perturbations. Park et al. (2019) suggest that as much as half the spheroidal component of disk dominated galaxies may arise from orbits aligned with the disk in this way. When we consider the fact that the galaxies in our sample are indeed disk-dominated with stellar masses comparable to those of local Milky Way-like galaxies, then it becomes plausible that the results of Bell et al. (2017), Park et al. (2019), and Wang et al. (2019) apply here, indicating that the bulge stellar mass that we can attribute purely to merger driven growth could be substantially less than the bulge stellar masses reported in Figure 6.1.

As such, if we consider the above to be true, then not only are the black holes these galaxies host overly massive compared to the canonical black hole-bulge relation, but the bulges themselves are overly massive compared to canonical frameworks for predicting bulge sizes based upon mergers.

We also investigate the relationship between black hole mass and total stellar mass, our results are displayed in the right panel of Figure 6.1. We note here that the fitted relation for the Häring & Rix (2004) data is unchanged in the right panel relative to the left. Häring & Rix (2004) do not perform bulge-disk decompositions for 29 of the 30 galaxies in their sample, and furthermore $\gtrsim 80\%$ of these galaxies are given a visual classification in de Vaucouleurs et al. (1991) of type E of S0. Hence, we make the assumption that $\mathrm{M_{Bulge}} \approx \mathrm{M_*}$ for each of the galaxies in the Häring & Rix (2004) sample.

For further comparison, we also include relations for early-type galaxies from McConnell & Ma (2013) (green dot dashed) and Greene et al. (2020) (purple dotted). Whilst the McConnell & Ma (2013) relation was originally reported in the context of a $\mathrm{M_{BH}}$ vs. $\mathrm{M_{Bulge}}$ relation, we make the same assumption as for the Häring & Rix (2004) sample stated above that $\mathrm{M_{Bulge}} \approx \mathrm{M_*}$ in the context of these bulge-dominated early-type galaxies.

The fitted lines for both disk-dominated (solid blue) and bulge-dominated (dashed red, dot dashed green, dotted purple) galaxies considered here are somewhat consistent with each other, though only to $\sim 3\sigma$ and with a very large degree of scatter. These findings are also somewhat contrasting to the results of Simmons et al. (2017) who found a significantly stronger correlation between these properties. Performing tests for correlation, we find a Spearman correlation coefficient of 0.31, and a Pearson correlation coefficient of 0.32. Such values indicate the presence of a correlation of similar strength to that found between bulge stellar mass and black hole mass for this sample. Such a correlation is fairly weak, and this is evident from the large amount of scatter present in our stellar mass distribution.

The fact that a correlation between stellar mass and black hole mass is found for both bulge-dominated early-type galaxies and the disk-dominated galaxies of our sample, but with significantly more scatter for the disk-dominated galaxies has interesting implications for black hole galaxy co-evolution. Kormendy & Ho (2013) put forward a scenario wherein black holes with $M_{BH} \leq 10^{8.5}$ $M_{\odot}$ at $z \leq 1.5$ exist primarily in disk-dominated galaxies where enough gas reaches the black hole to allow for modest AGN activity, but that this should be so stochastic in nature as to preclude the co-evolution of the black hole with its host galaxy.

The galaxies we consider in this sample host black holes with $M_{BH} \leq 5 \times 10^8$ $M_{\odot}$, and have been merger free since $z \sim 2$, and so should fit neatly into the picture outlined above. However, it is clear from the analysis we have conducted that the AGN activity in these objects is far from modest, and clearly some secular process is driving black hole growth in these systems at appreciable rates. The significantly increased scatter in the fitted relations for our disk-dominated sample lends more credibility to the picture presented by Kormendy & Ho (2013) that these secular growth processes are highly stochastic in nature, but the presence of correlation between black hole mass and stellar mass for our sample, however weak, implies that these processes are not stochastic enough to prohibit co-evolution.

Greene et al. (2020) also investigate the relationships between black hole mass and galaxy stellar mass for large populations of early-type and late-type galaxies. Their findings show a clear offset in the normalisation of the fitted relations for the different galaxy sub-samples, with late-type galaxies typically displaying lower stellar masses for a given black hole mass, and with more scatter. It is also noted that this scatter becomes more apparent at lower stellar masses ($M_* \lesssim 10^{11}$ $M_{\odot}$), particularly for late-type galaxies. These findings might help explain the observed scatter in stellar mass for our sample of disk-dominated galaxies, and could support the picture we present above wherein secular growth processes in disk-dominated galaxies increase the stochasticity of black hole-galaxy co-evolution, but do not preclude it.

We recognise that our stellar mass estimates differ significantly from those calculated in Simmons et al. (2017), and we attribute this primarily to changes in the SDSS pipeline from DR8 to DR16 (see Chapter 4.2) As we are making use of the most up to date SDSS Data Release, we make the argument that the $u-r$ colours (and hence mass-to-light ratios and galaxy stellar masses inferred from them) in this work are the most accurate in comparison to those of Simmons et al. (2017).

An alternate explanation for the the extreme large degree of scatter in our stellar masses is the method used to calculate them, detailed in Chapter 4.2. In removing the PSF contribution to the flux in the u and r bands by multiplying the flux by our calculated host-to-total luminosity ratios, we implicitly assume that the PSF contribution to galaxy flux is identical in both these bands. As the filters differ in central wavelength by ~ 2700Å this assumption will clearly have significant impacts on our ability to recover accurate PSF-corrected filter magnitudes. We note here however that Richards et al. (2006) show that the spectral energy distributions of Type I quasars should not vary significantly between 3543Å (u band) and 6231Å (r band) (see their Figure 10). Furthermore, when we investigate the `PSFmag` values for the u and r filters we find broadly similar values, with mean apparent mags in SDSS DR16 of 18.47 and 17.66 respectively. Regardless, any such issues in the above methodology are further compounded during the fitting process by the inherent 0.3 dex scatter in the colour-luminosity relation.

Additional *HST* imaging of each of these galaxies in a different filter would allow for a calculation of galaxy colour analogous to the $u - r$ colour from SDSS used to calculate mass-to-light ratios here. Taylor et al. (2011) make use of SDSS $g - i$ colours to estimate galaxy mass-to-light ratios to a precision of $\lesssim 0.1$ dex, a marked improvement over the 0.3 dex scatter from the $u - r$ colour relation implemented in this work. As such, given we have already obtained imaging of these galaxies in filters roughly corresponding to the SDSS i band, follow-up imaging in a filter such as F475W would provide information corresponding to the g band, and hence allow for more accurate estimation of galaxy mass-to-light ratios. This approach has the additional benefit that the *HST* PSF is extremely well studied, modelled and constrained, and hence the removal of the AGN component from these galaxies would be significantly more accurate, especially when we consider the ease of access to myriad parametric fitting programs including `GALFIT` which we make extensive use of here. Further, recent works such as Schombert et al. (2022) have also endeavoured to provide estimates of galaxy mass-to-light ratios that are additionally corrected for the presence of bulge and disk components, and such frameworks are invaluable when performing stellar mass estimates in samples such as ours.

Obtaining these improved stellar masses would allow further investigation into whether the scatter present in the right panel of Figure 6.1 is inherent and indicative of the galaxy co-evolution picture outlined above, or simply a result of our stellar mass estimation. This latter option leaves open the possibility of stronger correlations between stellar mass and black hole mass, such as those found in Simmons et al. (2017).

Chapter 7

Conclusion

By utilising high resolution *HST* imagery, we have performed comprehensive structural decomposition and analysis on a group of galaxies which are unambiguously disk-dominated, and hence have not participated in a major galaxy merger since redshift $z \sim 2$.

We find the majority of the components making up these galaxies lie below the Kormendy relation indicating they are rotation dominated in nature, and we find an average bulge-to-total luminosity ratio of 0.1 $\pm$ 0.1 for the entire sample, indicating the extremely low prevalence of classical bulges and dispersion supported structures within the galaxies considered. We find a mean bulge mass for those galaxies with detected bulges of $3 \times 10^9 \mathrm{M}_\odot$.

When considering the black hole masses of the sample, we investigate subsamples of galaxies which host only a pseudobulge, only a classical bulge, or neither pseudobulge nor classical bulge. We find evidence that galaxies hosting bulges also host more massive black holes, and that this trend is statistically significant to 2.9σ. However, we also report some of the highest black hole mass estimates of truly bulgeless galaxies in the literature, with a median black hole mass of galaxies hosting neither pseudobulge nor classical bulge in our sample of $2.9 \times 10^7 \mathrm{M}_\odot$. These findings indicate that whilst potential past mergers may enhance black hole growth in a given system, black holes can also grow to supermassive size through purely secular processes completely independent of major mergers.

Such findings are reinforced when we consider the Eddington fractions of our sub-samples, where we find no indication that galaxies hosting bulges have a statistically significantly higher fractional growth rate than those which have no bulge component, indicating black hole growth in the long term proceeds at comparable rates for both sub-samples.

We investigate the stellar masses of these sub-samples, and find little indication that galaxies hosting bulges have statistically significantly higher stellar masses, however such galaxies do seem to lack the low stellar mass tail exhibited by those galaxies hosting only pseudobulges, and the overall sample. This is potentially indicative that those galaxies hosting bulges in our sample tend to have stellar masses above a given mass threshold, and these findings may be consistent with galaxies hosting bulges residing in denser environments that can facilitate more star formation.

Furthermore, when we consider the bolometric AGN luminosity within our sample we find that galaxies which host bulge components but no pseudobulge components have higher overall luminosities, and that this difference is statistically significant to 2.3σ. Such findings suggest that galaxies which host bulges also host more luminous AGN which may be consistent with previous literature, though we note that the processes discussed occur on considerably different timescales. We also postulate that this increase in bolometric AGN luminosity may be related both to the increase in overall black hole mass and the lack of low stellar mass galaxies in the bulge-only sub-sample as reported above. If galaxies hosting bulges do indeed reside in denser environments (where they are more likely to have undergone a past merger to create the bulge component we detect), then perhaps the easier access to cool molecular gas this provides allows for both enhanced star formation and increased accretion onto the black hole, resulting in a more luminous AGN and a higher mass black hole. This hypothesis does have significant caveats however, principally the issue that the measured Eddington fractions of our objects display no preference for enhanced fractional growth rate among the bulge-only sample, and theoretical work which argues merger driven black hole fuelling should have the combined effect of limiting black hole growth and reducing AGN luminosity.

The above findings are evidence that whilst galaxy mergers might result in enhanced AGN luminosity, black hole mass and potentially galaxy stellar mass, they are unlikely to be the dominant process impacting black hole growth in the long term, as we find ample evidence in our sample that regardless of whether or not galaxies have been involved in a past merger, they can grow their black holes to significant and comparable mass in the local Universe. Further observational work, including an HI survey with an instrument such as the Institute for Radio Astronomy in the Millimetre Range (IRAM) 30m telescope would help to better probe the nature of the environments around these galaxies and determine the effect this may have on the sample parameters mentioned above.

We subsequently investigate the fraction of barred galaxies within our sample to ascertain the extent to which galaxy bars might help fuel black hole growth in the long term. We find the fraction of galaxies with bars within our sample ($25 \pm 0.3\%$) is consistent with the global bar fraction among disk galaxies at low redshift ($29.4 \pm 0.4\%$). When investigating bolometric AGN luminosity and black hole mass distributions for the barred galaxies we find both are in good agreement with the overall distribution of the sample, with tests for statistical significance indicating that the null hypothesis cannot be ruled out in any case. Such findings suggest that bars are merely one of many possible pathways for facilitating secular black hole growth, with some other mechanism common to all galaxies in our sample providing the majority of the fuel. As such, the presence of a bar is not a requirement to grow black holes to supermassive size in the local Universe in the absence of major mergers.

Finally, we investigate black hole galaxy co-evolution. We find evidence of correlation between bulge stellar mass and black hole mass for our sample of disk-dominated galaxies, though these correlations are weak and subject to significant scatter, as well as being somewhat inconsistent with the relation obtained from a sample of early-type galaxies which are representative of the canonical black-hole bulge relation. We note that a large and significant proportion of our disk-dominated galaxies have black holes which are overly massive compared to this canonical relation, and propose that the bulges themselves may be overly massive compared to estimates from purely merger-driven growth.

When considering total stellar mass versus black hole mass we find a correlation of similar strength to that of bulge stellar mass versus black hole mass, but again we note the significant scatter in our stellar mass values, as well as the fact that the fitted relation is only somewhat consistent with those derived for bulge-dominated early-type galaxies.

We note that that the fact that both of these correlations are present and of similar strength, and are significantly less strong that those found for elliptical galaxies has interesting implications for black hole galaxy co-evolution. We present a picture of co-evolution wherein the rich merger histories of early-type galaxies rigidly constrains how co-evolution proceeds, resulting in black holes and bulge masses which are tightly correlated. Conversely, the comparatively calm accretion histories of disk-dominated galaxies allow for a more stochastic co-evolution, explaining the more marked scatter in galaxy properties we observe for these objects.

However, we note this large degree of scatter could be a result of our method for stellar mass estimation and this combined with the inherent uncertainties in the colour-luminosity relation is likely to have a significant effect on our ability to determine any correlation between these two properties. We propose further observation with *HST* using a filter such as F475W to allow for an estimate of galaxy mass-to-light ratio utilising $g-i$ colours as outlined in Taylor et al. (2011) for SDSS sources in order to better determine the stellar masses of these galaxies, and re-evaluate the strength of the correlation between this property and black hole mass.

We also advocate for the construction of larger samples of local bulgeless and disk-dominated galaxies for structural decomposition. Such structural decomposition utilising high resolution imagery might allow further investigation of samples of disk-dominated galaxies that still host small classical bulges at their centres, and may help to determine whether our findings that such systems host overly luminous AGN and overly massive black holes is true for the global AGN fraction. Furthermore, such investigations may provide more detail on the dynamical nature of these small bulges, and help reveal whether a significant fraction of them were once "red nuggets", or whether they have indeed formed through galaxy mergers at high redshift. Such observations may also shed light on the extent to which secular processes have grown such classical bulges.

Finally, we recognise that the selection techniques implemented here preferentially select samples of the most luminous AGN, and as such these objects may represent the extreme tail of a distribution of black holes fuelled by primarily secular growth processes. As such, follow up work should aim to extend our findings into the more moderate luminosity regime giving us a better overall picture of the extent to which purely secular growth processes fuel black hole growth in the long term.

The vast survey area covered by the upcoming Vera C. Rubin Observatory (previously the Large Synoptic Survey Telescope, Ivezić et al., 2019) places it in a unique position to identify in the first instance these objects described above and to improve our overall catalogue sizes, whilst a combination of high resolution follow-up by both *HST* and the upcoming Euclid mission (Laureijs et al., 2011) will allow for final characterisation and structural decomposition to better investigate galaxy properties and components.

Appendix A

Column Name	Description
Galaxy_ID	Assigned DISKDOM galaxy ID
name	SDSS DR16 ID
RA	Galaxy Right Ascension (decimal)
Dec	Galaxy Declination (decimal)
RA_hms	Galaxy Right Ascension
Dec_dms	Galaxy Declination
z	Galaxy Redshift
z_source	Source for obtaining galaxy redshift
Filter	*HST* filter used to image galaxy
Magnitude_zeropoint	*HST* filter zeropoint (AB Magnitude)
Exposure_time	*HST* image exposure time (seconds)
Bolometric_Luminosity	Galaxy bolometric luminosity
PSF_x_coordinate	GALFIT fitted PSF x coordinate
PSF_y_coordinate	GALFIT fitted PSF y coordinate
PSF_magnitude	GALFIT fitted PSF magnitude
Component_x_type	Initially assigned component type for Component x (not utilising Kormendy Relation)
Component_x_new_type	Final assigned component type for Component x (utilising Kormendy Relation)
Component_x_magnitude	GALFIT fitted Component x magnitude
Component_x_surface_brightness	GALFIT fitted Component x surface brightness
Component_x_effective_radius	GALFIT fitted Component x effective radius
Component_x_sersic_index	GALFIT fitted Component x Sérsic index
Component_x_axis_ratio	GALFIT fitted Component x axis ratio
Component_x_position_angle	GALFIT fitted Component x position angle
Component_x_fourier_mode_amplitude	GALFIT fitted Component x Fourier Mode amplitude
Component_x_fourier_mode_phase_angle	GALFIT fitted Component x Fourier Mode phase angle
Component_x_Diskyness(-)/Boxyness(+)	GALFIT fitted Component x Diskyness/Boxyness parameter
Component_x_truncation_x_coordinate	GALFIT fitted Component x truncation x coordinate
Component_x_truncation_y_coordinate	GALFIT fitted Component x truncation y coordinate
Component_x_truncation_break_radius	GALFIT fitted Component x truncation break radius
Component_x_truncation_softening_length	GALFIT fitted Component x truncation softening length
Component_x_truncation_axis_ratio	GALFIT fitted Component x truncation axis ratio
Component_x_truncation_position_angle	GALFIT fitted Component x truncation position angle
Component_x_spiral_inner_radius	GALFIT fitted Component x spiral inner radius
Component_x_spiral_outer_radius	GALFIT fitted Component x spiral outer radius
Component_x_spiral_cumulative_rotation_to_outer_radius	GALFIT fitted Component x spiral cumulative rotation to outer radius
Component_x_asymptotic_spiral_power_law	GALFIT fitted Component x asymptotic spiral power law
Component_x_spiral_inclination_to_L.O.S.	GALFIT fitted Component x spiral inclination to L.O.S.
Component_1_spiral_sky_position_angle	GALFIT fitted Component x spiral sky position angle
Total_Galaxy_Luminosity	Total galaxy luminosity (including PSF contribution)
Total_Galaxy_Luminosity_Min	Minimum total galaxy luminosity (including PSF contribution) using errors from GALFIT fits
Total_Galaxy_Luminosity_Max	Maximum total galaxy luminosity (inluding PSF contribution) using errors from GALFIT fits
Total_Host_Galaxy_Luminosity	Total galaxy luminosity (excluding PSF contribution)
Total_Host_Galaxy_Luminosity_Min	Minimum total galaxy luminosity (excluding PSF contribution) using errors from GALFIT fits
Total_Host_Galaxy_Luminosity_Max	Maximum total galaxy luminosity (excluding PSF contribution) using errors from GALFIT fits
PSF_Luminosity	Galaxy PSF luminosity
PSF_Luminosity_Ratio	Galaxy PSF luminosity ratio (PSF_Luminosity / Total_Host_Galaxy_Luminosity)
PSF_Luminosity_Ratio_Min	Minimum galaxy PSF luminosity ratio
PSF_Luminosity_Ratio_Max	Maximum galaxy PSF luminosity ratio
Bulge_Luminosity_Ratio	Galaxy bulge luminosity ratio (Total Bulge Luminosity / Total_Host_Galaxy_Luminosity)
Bulge_Luminosity_Ratio_Min	Minimum galaxy bulge luminosity ratio
Bulge_Luminosity_Ratio_Max	Maximum galaxy bulge luminosity ratio
Pseudobulge_Luminosity_Ratio	Galaxy pseudobulge luminosity ratio (Total Pseudobulge Luminosity / Total_Host_Galaxy_Luminosity)
Pseudobulge_Luminosity_Ratio_Min	Minimum galaxy pseudobulge luminosity ratio
Pseudobulge_Luminosity_Ratio_Max	Maximum galaxy pseudobulge luminosity ratio
Compact_Component_Luminosity_Ratio	Galaxy compact component luminosity ratio (Total Bulge Luminosity + Total Pseudobulge Luminosity / Total_Host_Galaxy_Luminosity)
Compact_Component_Luminosity_Ratio_Min	Minimum galaxy compact component luminosity ratio
Compact_Component_Luminosity_Ratio_Max	Maximum galaxy compact component luminosity ratio
upmag_cone	SDSS DR16 galaxy PSF magnitude (u band)
rpmag_cone	SDSS DR16 galaxy PSF magnitude (r band)
e_upmag_cone	SDSS DR16 galaxy PSF magnitude error (u band)
e_rpmag_cone	SDSS DR16 galaxy PSF magnitude error (r band)
umag	SDSS DR16 galaxy magnitude (u band)
rmag	SDSS DR16 galaxy magnitude (r band)
e_umag	SDSS DR16 galaxy magnitude error (u band)
e_rmag	SDSS DR16 galaxy magnitude error (r band)
Stellar_Mass	Galaxy stellar mass (using SDSS DR16 u-r colours)
Err_Stellar_Mass	Galaxy stellar mass error (using SDSS DR16 u-r colours)
MBH	Galaxy black hole mass (for information regarding black hole mass calculations we refer to Simmons et al. (2017))
Err_MBH	Galaxy black hole mass error (for information regarding black hole mass calculations we refer to Simmons et al. (2017))

Table A.1 *HST* structural parameters from decomposition using `GALFIT`. x refers to the component number, and varies in our sample from 1 to 5. For more information regarding the GALFIT fitted components we refer to the GALFIT documenation (Peng et al., 2002, 2010). Table available in online electronic version at: `https://github.com/mjfahey99/DISKDOM-Catalogue`.

References

Ahn C. P., et al., 2012, The Astophysical Journal Supplement Series, 203, 21

Ahumada R., et al., 2020, The Astophysical Journal Supplement Series, 249, 3

Allevato V., et al., 2011, The Astrophysical Journal, 736, 99

Ann H. B., Thakur P., 2005, The Astrophysical Journal, 620, 197

Astropy Collaboration et al., 2013, Astronomy and Astrophysics, 558, A33

Athanassoula E., 2003, Monthly Notices of the Royal Astronomical Society, 341, 1179

Baldry I. K., Balogh M. L., Bower R. G., Glazebrook K., Nichol R. C., Bamford S. P., Budavari T., 2006, Monthly Notices of the Royal Astronomical Society, 373, 469

Barnes J. E., Hernquist L., 1996, The Astrophysical Journal, 471, 115

Bell E. F., Monachesi A., Harmsen B., de Jong R. S., Bailin J., Radburn-Smith D. J., D'Souza R., Holwerda B. W., 2017, The Astrophysical Journal Letters, 837, L8

Bessiere P. S., Tadhunter C. N., Ramos Almeida C., Villar Martín M., 2014, Monthly Notices of the Royal Astronomical Society, 438, 1839

Bohn T., Canalizo G., Satyapal S., Pfeifle R. W., 2020, The Astrophysical Journal, 899, 82

Bohn T., Canalizo G., Satyapal S., Sales L. V., 2022, The Astrophysical Journal, 931, 69

Brook C. B., Stinson G., Gibson B. K., Roškar R., Wadsley J., Quinn T., 2012, Monthly Notices of the Royal Astronomical Society, 419, 771

Cheung E., et al., 2015, Monthly Notices of the Royal Astronomical Society, 447, 506

Cisternas M., et al., 2011, The Astrophysical Journal Letters, 741, L11

Cisternas M., Sheth K., Salvato M., Knapen J. H., Civano F., Santini P., 2015, The Astrophysical Journal, 802, 137

Costantin L., et al., 2020, The Astrophysical Journal Letters, 889, L3

Croton D. J., et al., 2006, Monthly Notices of the Royal Astronomical Society, 365, 11

D'Onghia E., Vogelsberger M., Hernquist L., 2013, The Astrophysical Journal, 766, 34

Damjanov I., et al., 2009, The Astrophysical Journal, 695, 101

Davies R. I., Maciejewski W., Hicks E. K. S., Tacconi L. J., Genzel R., Engel H., 2009, The Astrophysical Journal, 702, 114

Donner K. J., Thomasson M., 1994, Astronomy and Astrophysics, 290, 785

Dunlop J. S., McLure R. J., Kukula M. J., Baum S. A., O'Dea C. P., Hughes D. H., 2003, Monthly Notices of the Royal Astronomical Society, 340, 1095

Edelson R., Malkan M., 2012, The Astrophysical Journal, 751, 52

Ellison S. L., Mendel J. T., Patton D. R., Scudder J. M., 2013, Monthly Notices of the Royal Astronomical Society, 435, 3627

Elvis M., Risaliti G., Zamorani G., 2002, The Astrophysical Journal Letters, 565, L75

Emsellem E., et al., 2011, Monthly Notices of the Royal Astronomical Society, 414, 888

Ferrarese L., Merritt D., 2000, The Astrophysical Journal Letters, 539, L9

Fisher D. B., Drory N., 2008, The Astronomical Journal, 136, 773

Friedli D., Benz W., 1993, Astronomy and Astrophysics, 268, 65

Gabor J. M., et al., 2009, The Astrophysical Journal, 691, 705

Gadotti D. A., 2008, Monthly Notices of the Royal Astronomical Society, 384, 420

Galloway M. A., et al., 2015, Monthly Notices of the Royal Astronomical Society, 448, 3442

Gao F., et al., 2020, Astronomy and Astrophysics, 637, A94

Georgakakis A., et al., 2009, Monthly Notices of the Royal Astronomical Society, 397, 623

Glikman E., Simmons B., Mailly M., Schawinski K., Urry C. M., Lacy M., 2015, The Astrophysical Journal, 806, 218

Goulding A. D., et al., 2017, The Astrophysical Journal, 843, 135

Greene J. E., Ho L. C., 2005, The Astrophysical Journal, 630, 122

Greene J. E., et al., 2010, The Astrophysical Journal, 721, 26

Greene J. E., Strader J., Ho L. C., 2020, Annual Review of Astronomy and Astrophysics, 58, 257

Grogin N. A., et al., 2005, The Astrophysical Journal Letters, 627, L97

Guo M., Du M., Ho L. C., Debattista V. P., Zhao D., 2020, The Astrophysical Journal, 888, 65

Hamabe M., Kormendy J., 1987, in de Zeeuw P. T., ed., Vol. 127, Structure and Dynamics of Elliptical Galaxies. p. 379, doi:10.1007/978-94-009-3971-4_32

Häring N., Rix H.-W., 2004, The Astrophysical Journal Letters, 604, L89

Hasinger G., Miyaji T., Schmidt M., 2005, Astronomy and Astrophysics, 441, 417

Hernquist L., 1989, Nature, 340, 687

Hopkins P. F., Quataert E., 2010, Monthly Notices of the Royal Astronomical Society, 407, 1529

Hopkins P. F., Somerville R. S., Hernquist L., Cox T. J., Robertson B., Li Y., 2006, The Astrophysical Journal, 652, 864

Hopkins P. F., Cox T. J., Younger J. D., Hernquist L., 2009, The Astrophysical Journal, 691, 1168

Hopkins P. F., Kereš D., Murray N., Quataert E., Hernquist L., 2012, Monthly Notices of the Royal Astronomical Society, 427, 968

Hunt J. A. S., Hong J., Bovy J., Kawata D., Grand R. J. J., 2018, Monthly Notices of the Royal Astronomical Society, 481, 3794

Hunter J. D., 2007, Computing In Science & Engineering, 9, 90

Ivezić Ž., et al., 2019, The Astrophysical Journal, 873, 111

Jiang Y.-F., Greene J. E., Ho L. C., Xiao T., Barth A. J., 2011, The Astrophysical Journal, 742, 68

Jones E., Oliphant T., Peterson P., et al., 2001, SciPy: Open source scientific tools for Python, `http://www.scipy.org/`

Kannan R., Macciò A. V., Fontanot F., Moster B. P., Karman W., Somerville R. S., 2015, Monthly Notices of the Royal Astronomical Society, 452, 4347

Keel W. C., et al., 2012, The Astronomical Journal, 144, 66

Kereš D., Katz N., Weinberg D. H., Davé R., 2005, Monthly Notices of the Royal Astronomical Society, 363, 2

Kim M., Ho L. C., Peng C. Y., Barth A. J., Im M., 2008, The Astophysical Journal Supplement Series, 179, 283

Knapen J. H., Shlosman I., Peletier R. F., 2000, The Astrophysical Journal, 529, 93

Kocevski D. D., et al., 2012, The Astrophysical Journal, 744, 148

Kormendy J., 1977, The Astrophysical Journal, 218, 333

Kormendy J., Bender R., 2011, Nature, 469, 377

Kormendy J., Gebhardt K., 2001, in Wheeler J. C., Martel H., eds, American Institute of Physics Conference Series Vol. 586, 20th Texas Symposium on relativistic astrophysics. pp 363–381 (arXiv:astro-ph/0105230), doi:10.1063/1.1419581

Kormendy J., Ho L. C., 2013, Annual Review of Astronomy and Astrophysics, 51, 511

Kormendy J., Kennicutt Robert C. J., 2004, Annual Review of Astronomy and Astrophysics, 42, 603

Kormendy J., Drory N., Bender R., Cornell M. E., 2010, The Astrophysical Journal, 723, 54

Kormendy J., Bender R., Cornell M. E., 2011, Nature, 469, 374

Laine S., Shlosman I., Knapen J. H., Peletier R. F., 2002, The Astrophysical Journal, 567, 97

Laureijs R., et al., 2011, arXiv e-prints, p. arXiv:1110.3193

Laurikainen E., Salo H., Buta R., 2004, The Astrophysical Journal, 607, 103

Lee G.-H., Woo J.-H., Lee M. G., Hwang H. S., Lee J. C., Sohn J., Lee J. H., 2012, The Astrophysical Journal, 750, 141

Lin L.-H., Wang H.-H., Hsieh P.-Y., Taam R. E., Yang C.-C., Yen D. C. C., 2013, The Astrophysical Journal, 771, 8

Maciejewski W., 2004, Monthly Notices of the Royal Astronomical Society, 354, 892

Maciejewski W., Teuben P. J., Sparke L. S., Stone J. M., 2002, Monthly Notices of the Royal Astronomical Society, 329, 502

Magorrian J., et al., 1998, The Astronomical Journal, 115, 2285

Marconi A., Hunt L. K., 2003, The Astrophysical Journal Letters, 589, L21

Marian V., et al., 2019, The Astrophysical Journal, 882, 141

Marleau F. R., Clancy D., Bianconi M., 2013, Monthly Notices of the Royal Astronomical Society, 435, 3085

Martig M., Bournaud F., Croton D. J., Dekel A., Teyssier R., 2012, The Astrophysical Journal, 756, 26

Martin G., et al., 2018, Monthly Notices of the Royal Astronomical Society, 476, 2801

Martini P., Regan M. W., Mulchaey J. S., Pogge R. W., 2003, The Astrophysical Journal, 589, 774

Masters K. L., et al., 2011, Monthly Notices of the Royal Astronomical Society, 411, 2026

McAlpine S., Harrison C. M., Rosario D. J., Alexander D. M., Ellison S. L., Johansson P. H., Patton D. R., 2020, Monthly Notices of the Royal Astronomical Society, 494, 5713

McConnell N. J., Ma C.-P., 2013, , 764, 184

Miller R. H., Smith B. F., 1979, The Astrophysical Journal, 227, 785

Nigoche-Netro A., Ruelas-Mayorga A., Franco-Balderas A., 2008, Astronomy and Astrophysics, 491, 731

Oh S., Oh K., Yi S. K., 2012, The Astophysical Journal Supplement Series, 198, 4

Oke J. B., Gunn J. E., 1983, The Astrophysical Journal, 266, 713

Park M.-J., et al., 2019, The Astrophysical Journal, 883, 25

Peng C. Y., 2007, The Astrophysical Journal, 671, 1098

Peng C. Y., Ho L. C., Impey C. D., Rix H.-W., 2002, The Astronomical Journal, 124, 266

Peng C. Y., Ho L. C., Impey C. D., Rix H.-W., 2010, The Astronomical Journal, 139, 2097

Pierce C. M., et al., 2010, Monthly Notices of the Royal Astronomical Society, 405, 718

Pontzen A., Tremmel M., Roth N., Peiris H. V., Saintonge A., Volonteri M., Quinn T., Governato F., 2017, Monthly Notices of the Royal Astronomical Society, 465, 547

Regan M. W., Teuben P. J., 2004, The Astrophysical Journal, 600, 595

Richards G. T., et al., 2006, The Astophysical Journal Supplement Series, 166, 470

Rosario D. J., et al., 2015, Astronomy and Astrophysics, 573, A85

Sakamoto K., 1996, The Astrophysical Journal, 471, 173

Sales L. V., Navarro J. F., Theuns T., Schaye J., White S. D. M., Frenk C. S., Crain R. A., Dalla Vecchia C., 2012, Monthly Notices of the Royal Astronomical Society, 423, 1544

Sancisi R., Fraternali F., Oosterloo T., van der Hulst T., 2008, The Astronomy and Astrophysics Review, 15, 189

Sanders D. B., Soifer B. T., Elias J. H., Madore B. F., Matthews K., Neugebauer G., Scoville N. Z., 1988, The Astrophysical Journal, 325, 74

Satyapal S., Vega D., Dudik R. P., Abel N. P., Heckman T., 2008, The Astrophysical Journal, 677, 926

Satyapal S., Böker T., Mcalpine W., Gliozzi M., Abel N. P., Heckman T., 2009, The Astrophysical Journal, 704, 439

Scannapieco C., White S. D. M., Springel V., Tissera P. B., 2009, Monthly Notices of the Royal Astronomical Society, 396, 696

Schawinski K., Dowlin N., Thomas D., Urry C. M., Edmondson E., 2010, The Astrophysical Journal Letters, 714, L108

Schawinski K., Treister E., Urry C. M., Cardamone C. N., Simmons B., Yi S. K., 2011, The Astrophysical Journal Letters, 727, L31

Schawinski K., Simmons B. D., Urry C. M., Treister E., Glikman E., 2012, Monthly Notices of the Royal Astronomical Society, 425, L61

Schawinski K., Koss M., Berney S., Sartori L. F., 2015, Monthly Notices of the Royal Astronomical Society, 451, 2517

Schlegel D. J., Finkbeiner D. P., Davis M., 1998, The Astrophysical Journal, 500, 525

Schnorr-Müller A., Storchi-Bergmann T., Nagar N. M., Ferrari F., 2014, Monthly Notices of the Royal Astronomical Society, 438, 3322

Schombert J., McGaugh S., Lelli F., 2022, The Astronomical Journal, 163, 154

Secrest N. J., Satyapal S., Gliozzi M., Cheung C. C., Seth A. C., Böker T., 2012, The Astrophysical Journal, 753, 38

Sersic J. L., 1968, Atlas de Galaxias Australes

Shen Y., et al., 2011, The Astophysical Journal Supplement Series, 194, 45

Shlosman I., Frank J., Begelman M. C., 1989, Nature, 338, 45

Silva A., Marchesini D., Silverman J. D., Martis N., Iono D., Espada D., Skelton R., 2021, The Astrophysical Journal, 909, 124

Simard L., Mendel J. T., Patton D. R., Ellison S. L., McConnachie A. W., 2011, The Astophysical Journal Supplement Series, 196, 11

Simmons B. D., Urry C. M., 2008, The Astrophysical Journal, 683, 644

Simmons B. D., Van Duyne J., Urry C. M., Treister E., Koekemoer A. M., Grogin N. A., GOODS Team 2011, The Astrophysical Journal, 734, 121

Simmons B. D., et al., 2013, Monthly Notices of the Royal Astronomical Society, 429, 2199

Simmons B. D., Smethurst R. J., Lintott C., 2017, Monthly Notices of the Royal Astronomical Society, 470, 1559

Skibba R. A., et al., 2012, Monthly Notices of the Royal Astronomical Society, 423, 1485

Smethurst R. J., Simmons B. D., Lintott C. J., Shanahan J., 2019, Monthly Notices of the Royal Astronomical Society, 489, 4016

Sparke L. S., Sellwood J. A., 1987, Monthly Notices of the Royal Astronomical Society, 225, 653

Sparre M., Springel V., 2017, Monthly Notices of the Royal Astronomical Society, 470, 3946

Tacchella S., Dekel A., Carollo C. M., Ceverino D., DeGraf C., Lapiner S., Mandelker N., Primack J. R., 2016, Monthly Notices of the Royal Astronomical Society, 458, 242

Taylor M., 2013, Starlink User Note, 253

Taylor E. N., et al., 2011, Monthly Notices of the Royal Astronomical Society, 418, 1587

Tonini C., Mutch S. J., Croton D. J., Wyithe J. S. B., 2016, Monthly Notices of the Royal Astronomical Society, 459, 4109

Trakhtenbrot B., Lira P., Netzer H., Cicone C., Maiolino R., Shemmer O., 2017, The Astrophysical Journal, 836, 8

Treister E., Schawinski K., Urry C. M., Simmons B. D., 2012, The Astrophysical Journal Letters, 758, L39

Urrutia T., Lacy M., Becker R. H., 2008, The Astrophysical Journal, 674, 80

Van Der Walt S., Colbert S. C., Varoquaux G., 2011, Computing in Science & Engineering, 13, 22

Volonteri M., Rees M. J., 2006, The Astrophysical Journal, 650, 669

Walker I. R., Mihos J. C., Hernquist L., 1996, The Astrophysical Journal, 460, 121

Wang L., et al., 2019, Monthly Notices of the Royal Astronomical Society, 482, 5477

Welker C., Dubois Y., Devriendt J., Pichon C., Kaviraj S., Peirani S., 2017, Monthly Notices of the Royal Astronomical Society, 465, 1241

Woo J.-H., Urry C. M., 2002, The Astrophysical Journal, 579, 530

Wright E. L., 2006, , 118, 1711

York D. G., et al., 2000, The Astronomical Journal, 120, 1579

Zolotov A., et al., 2015, Monthly Notices of the Royal Astronomical Society, 450, 2327

de Vaucouleurs G., 1953, Monthly Notices of the Royal Astronomical Society, 113, 134

de Vaucouleurs G., de Vaucouleurs A., Corwin Herold G. J., Buta R. J., Paturel G., Fouque P., 1991, Third Reference Catalogue of Bright Galaxies

de la Rosa I. G., La Barbera F., Ferreras I., Sánchez Almeida J., Dalla Vecchia C., Martínez-Valpuesta I., Stringer M., 2016, Monthly Notices of the Royal Astronomical Society, 457, 1916